PUCRS

School of Technology
Graduate Program in Electrical Engineering
Master's Degree in Electrical Engineering

MATHEUS SENNA DE OLIVEIRA

RESONANT GAIN SCHEDULING CONTROLLER FOR SPIRAL SCANNING PATTERNS IN ATOMIC FORCE MICROSCOPY

Porto Alegre
2018

PÓS-GRADUAÇÃO - *STRICTO SENSU*

Pontifícia Universidade Católica
do Rio Grande do Sul

Matheus Senna de Oliveira

Resonant Gain Scheduling Controller for Spiral Scanning Patterns in Atomic Force Microscopy

Master degree dissertation presented to the Graduate Program in Electric Engineering of the Pontifícia Universidade Católica do Rio Grande do Sul, as requisite to obtain the title of Master's Degree in Electrical Engineering.
Concentration Area: Signals, Systems and Information Technology
Research Line: Automation and Systems.

Pontifícia Universidade Católica do Rio Grande do Sul – PUCRS

School of Technology

Graduate Program in Electric Engineering

Supervisor: Aurélio Tergolina Salton

Porto Alegre - RS, Brazil

2018

Ficha Catalográfica

O48r Oliveira, Matheus Senna de

Resonant gain scheduling controller for spiral ccanning patterns in Atomic Force Microscopy / Matheus Senna de Oliveira . – 2018.

77 f.

Dissertação (Mestrado) – Programa de Pós-Graduação em Engenharia Elétrica, PUCRS.

Orientador: Prof. Dr. Aurélio Tergolina Salton.

1. Microscopia de Força Atômica. 2. Princípio do Modelo Interno. 3. seguimento de referência variante no tempo. 4. Controle Robusto. 5. Controle por Aprendizagem Iterativa. I. Salton, Aurélio Tergolina. II. Título.

Elaborada pelo Sistema de Geração Automática de Ficha Catalográfica da PUCRS
com os dados fornecidos pelo(a) autor(a).
Bibliotecário responsável: Marcelo Votto Texeira CRB-10/1974

Pontifícia Universidade Católica do Rio Grande do Sul
ESCOLA POLITÉCNICA
PROGRAMA DE PÓS-GRADUAÇÃO EM ENGENHARIA ELÉTRICA - PPGEE

RESONANT GAIN SCHEDULING CONTROLLER FOR SPIRAL SCANNING PATTERNS IN ATOMIC FORCE MICROSCOPY

CANDIDATO: MATHEUS SENNA DE OLIVEIRA

Esta Dissertação de Mestrado foi julgada para obtenção do título de MESTRE EM ENGENHARIA ELÉTRICA e aprovada em sua forma final pelo Programa de Pós-Graduação em Engenharia Elétrica da Pontifícia Universidade Católica do Rio Grande do Sul.

DR. AURELIO TERGOLINA SALTON - ORIENTADOR

BANCA EXAMINADORA

DR. DANIEL FERREIRA COUTINHO - PROGRAMA DE PÓS-GRADUAÇÃO EM ENGENHARIA DE AUTOMAÇÃO E SISTEMAS - UFSC

DRA. LETÍCIA MARIA BOLZANI PÖEHLS - PROGRAMA DE PÓS-GRADUAÇÃO EM ENGENHARIA ELÉTRICA - PUCRS

Agradecimentos

Primeiramente, eu gostaria de agradecer ao meu orientador, Prof. Aurélio Tergolina Salton, pelo conceito inicial do trabalho e pelas incontáveis sugestões e auxílios durante a elaboração do mesmo.

Agradeço também aos meus colegas, cujas amizades durante o curso de mestrado me ajudaram nas mais diversas situações.

Finalmente, um agradecimento especial a minha família, que passou por momentos difíceis ao longo do mestrado, mas sempre esteve ao meu lado me incentivando e dando o apoio necessário para seguir em frente.

Abstract

This document presents a dissertation work regarding the study of control strategies for the efficient tracking of spiral patterns. Such patterns arise in many areas, as for example the Atomic Force Microscopy, where fast and smooth reference signals are required. In order to successfully track the above mentioned references, which are composed of amplitude and frequency-varying sinusoidal signals, advanced control strategies were investigated. The Internal Model Principle is a traditional approach to track reference signals, but it cannot be directly applied in frequency-varying signals. Therefore, the present work proposed a robust control strategy where the Internal Model Principle was applied as a Resonant Control in an augmented time-varying structure. The augmented system and the reference frequency values were organized using a polytopic representation and structured as an optimization problem subject to constraints in the form of Linear Matrix Inequalities. This synthesis was evaluated through a set of simulations, using a numerical model of an Atomic Force Microscope and a new suitable scanning reference pattern. Moreover, using the premise that the same reference signals are tracked multiple times, an Iterative Learning Controller was also designed in order to improve the tracking performance of the proposed main strategy. Numerical results demonstrated that the designed controller achieved satisfactory results, in comparison to the traditional controller available in the area.

Keywords: Atomic Force Microscopy, Internal Model Principle, time-varying reference tracking, Robust Control, Iterative Learning Control.

Resumo

Este documento apresenta um trabalho de dissertação sobre o estudo de estratégias de controle para o seguimento eficiente de padrões espirais. Estes padrões podem ser aplicados em muitas áreas, como por exemplo, a Microscopia de Força Atômica, onde padrões de referenciais rápidos e suaves são requeridos. Para realizar com sucesso o seguimento destas referências, que são compostas de sinais senoidais de amplitude e frequência variável, estratégias de controle avançadas foram investigadas. O Princípio do Modelo Interno é uma abordagem tradicional para o seguimento de sinais, mas ele não pode ser aplicado diretamente em sinais com frequência variante. Logo, o presente trabalho propôs uma estratégia de controle robusto onde o Princípio do Modelo Interno foi aplicado como um Controlador Ressonante em uma estrutura aumentada e variante no tempo. O sistema aumentado e os valores da frequência foram organizados usando uma representação politópica e estruturados como um problema de otimização sujeito a restrições na forma de Desigualdades Matriciais Lineares. Esta síntese foi avaliada através de um conjunto de simulações, usando um modelo numérico de um Microscópio de Força Atômica e um novo padrão de referência para escaneamento apropriado. Além disso, usando a premissa que estes sinais de referência são aplicados múltiplas vezes, um Controle por Aprendizagem Iterativa também foi projetado para melhorar o desempenho do seguimento da estratégia principal proposta. Resultados numéricos demonstraram que o controlador projetado atingiu resultados satisfatórios, em comparação com o controlador tradicional disponível na área.

Palavras-chave: microscopia de força atômica, Princípio do Modelo Interno, seguimento de referência variante no tempo, Controle Robusto, Controle por Aprendizagem Iterativa.

List of figures

List of tables

List of abbreviations and acronyms

AFM	Atomic Force Microscopy
BIBO	Bounded Input-Bounded Output
CAV	Constant Angular Velocity
CLV	Constant Linear Velocity
DOF	Degree of Freedom
DSP	Digital Signal Processor
ILC	Iterative Learning Control
IMC	Internal Model Control
IMP	Internal Model Principle
KF	Kalman Filter
LMI	Linear Matrix Inequality
MEMS	Microelectromechanical System
MPC	Model Predictive Control
MRC	Multiple Resonant Controller
OPT	Optimal Archimedean Spiral
PI	Proportional-Integral
PID	Proportional-Integral-Derivative
RC	Resonant Controller
RMS	Root-Mean-Square
SISO	Single-Input Single-Output
SPM	Scanning Probe Microscopy

List of symbols

I_n	identity matrix with n lines and columns
$0_{n\times m}$	zeros matrix with n lines and m columns
$1_{n\times m}$	ones matrix with n lines and m columns
$A^\intercal$	transpose of the matrix A
$\star$	respective transposed element of a symmetric matrix, i.e., $\begin{bmatrix} A & B \\ \star & C \end{bmatrix} = \begin{bmatrix} A & B \\ B^\intercal & C \end{bmatrix}$
$\otimes$	Kronecker product
$\dot{x}(t)$	derivative of $x(t)$ with respect to time, i.e., $dx(t)/dt$
$f'(t_*)$	derivative of $f(t_*)$ with respect to the normalized time t_*
$\Delta x(k)$	discrete signal $x(k)$ variation, i.e., $x(k+1) - x(k)$
$\mathbb{C}$	set of complex numbers
$\mathbb{R}$	set of real numbers
$\mathbb{Z}_+$	set of positive integer numbers
$\gg$	if $a \gg b$, then a much greater than b
$\square$	end of the proof

Contents

1 Introduction

Reference tracking of time-varying signals is a traditional problem in the control area. Robotic manipulators (JIN, 2016), atomic force microscopes (BAZAEI et al., 2016) and frequency inverters (RAMOS; SOTO-PEREZ; CIFUENTES, 2017) are examples of applications where the system output must track a reference signal that varies over time. Fast convergence and small tracking error are common performance standards in these types of applications.

In the case of the Atomic Force Microscopy (AFM), for example, the performance is a critical item for the controller design. Atomic force microscopes are tools used in order to analyze materials in the scale of nanometers (BARÓ; REIFENBERGER, 2012). The final result of these equipments are images of the material structure. The scanning of samples in this small scale is highly susceptible to the presence of tracking errors or noise, which could compromise the image quality (HABIBULLAH; POTA; PETERSEN, 2014b). During the last few years, different approaches were developed in order to improve AFM scans, such as the project of the scanning pattern used by the microscope (MAHMOOD; MOHEIMANI, 2010).

There are many different patterns for the AFM scanning. The most basic one is the raster scanning pattern, usually found in atomic force microscopes (YABLON, 2014). Among many different patterns, such as the cycloid and Lissajous (TUMA et al., 2013), we may highlight the Archimedean spiral pattern. In this pattern, the distance between the loops, i.e., the distance between the curves that compose the spiral, is constant, which allows a homogeneous scanning without over-imaging (RANA; POTA; PETERSEN, 2014).

In comparison to the raster scanning pattern the spiral pattern allows higher velocities and robustness to noise (MAHMOOD; MOHEIMANI; BHIKKAJI, 2011). Nevertheless, the spiral pattern has its own difficulties. They are generated using two sinusoidal signals, each one applied in one of the two microscope horizontal planes. These references, which can have varying frequency and amplitude, require more sophisticated tracking control strategies in order to achieve satisfactory performance.

Besides the AFM area, there are more applications where the problem of spiral reference tracking is relevant. Two main examples are the Fiber Scanners (LEE et al., 2010) and the Pico-Projectors (SCHOWENGERDT et al., 2009). In medical imaging area, the Fiber Scanners play an important role for the surface-based techniques using optical endoscopes. According to Lee et al. (2010), this equipment allows "high quality laser-based imaging within an ultrathin and flexible endoscope", which can be achieved using spiral patterns. The Pico-Projectors are useful in the context of technological miniaturization

of electronic gadgets, like laptops and smartphones. As presented in Schowengerdt et al. (2009), nano fiber-coupled laser diodes use the spiral pattern in order to project light, which may be used for gaming, movies transmission and video conferencing.

One of the more traditional strategies in order to realize reference tracking is the so-called Internal Model Principle (IMP) (FRANCIS; WONHAM, 1976). The IMP establishes that if the exogenous system dynamic is placed in the controller loop, then the tracking is guaranteed in steady state. For example, considering a step signal as the reference, the controller must add an integrator in the control loop in order to achieve asymptotic tracking. When the reference is a sinusoidal signal, then the IMP is applied through the Resonant Controller (RC) (CHEN, 1999).

If the reference signal is composed of multiple known frequencies values, then the Multiple Resonant Controller (MRC) is a suitable option (PEREIRA et al., 2014). The MRC consists in a set of resonant controllers, each one designed for one of the reference signal frequencies. As any periodic signal may be rewritten as a weighted sum of sine and cosine functions through the Fourier series expansion, the MRC may be applied to a wide range of periodic references.

Nevertheless, there are situations where the reference frequency may not be limited to a single value or a small set of values. Taking for example the previously cited AFM, its spiral scanning patterns may be generated through amplitude and frequency-varying sinusoidal signals (ZIEGLER et al., 2017), composed by a considerable interval of values. Therefore, the direct application of the IMP through the RC is not viable in this situation. Even the MRC would require a very large number of modes to achieve satisfactory tracking. Therefore, other control strategies must be used in order to track these references using the IMP.

Habibullah, Pota e Petersen (2014b) used a resonant controller in order for spiral reference tracking in AFM. Nevertheless, all the tracked spirals only had constant frequency. Bazaei, Maroufi e Moheimani (2017) proposed a controller to track frequency-varying spirals, but in this case the resonant controller was used only to upgrade a feedforward gain. Das, Pota e Petersen (2012) used a resonant controller in an AFM application, but for the tracking of a triangular wave for a raster scanning pattern. Preliminary results of the present dissertation can be found in (OLIVEIRA; SALTON; FLORES, 2017), where an optimal frequency-varying resonant controller was proposed for a frequency-varying spiral pattern. The control structure was organized in such a way that the feedback gains are computed by the Linear Quadratic Regulator.

Others control used for spiral reference tracking were Model Predictive Control (MPC) (RANA; POTA; PETERSEN, 2015) and Internal Model Control (IMC) (MAHMOOD; MOHEIMANI, 2010). The MPC is an optimal control technique, that uses numerical optimization in order to define the current control input based in the system

future responses. The IMC, which also is based on the IMP, uses the system model explicitly as a part of the controller in order to deal with any uncertainty regarding the real plant.

Robust control is another important research topic in this context. It is a method for solving control problems involving a nominal system and a family of uncertainties around it (BOYD, 1994). One example is the design of controllers for time-varying systems, where the parameters variation must be considered in the problem. In this context, the state-space approach using polytopic modeling is an interesting strategy, where the problems may be designed using Lyapunov functions (BERNUSSOU; PERES; GEROMEL, 1990) and Linear Matrix Inequalities (LMIs) structures.

The feedforward controllers are another suitable option in reference tracking. The feedforward strategy makes use of the reference measure in order to take action before it the signal affects the system (ŻAK, 2003). There are many ways to apply this concept. For example, it is possible to compensate the system gain in order to better track the reference signal. Another feedforward approach is the Iterative Learning Control (ILC).

In this strategy, the information obtained in previous batches is used in the next executions, in order to improve the tracking performance (BRISTOW; THARAYIL; ALLEYNE, 2006). Considering the context of the current work, where the scanning of samples may be performed using the same reference pattern in multiple batches in order to, for example, generate a video recording of the scanned sample, the ILC becomes an interesting option. More than a direct solution for the control of a system, the Iterative Learning Control is mostly applied along side with a feedback controller, in order to improve the general performance over the repeated tasks (BOEREN et al., 2016).

The ILC was previously applied for AFM scanning patterns tracking, but as far as the author knows, it was not for the frequency-varying spirals case. Butterworth, Pao e Abramovitch (2011) applied the ILC was used for x-y axes reference tracking, but for triangular waves that compose the raster pattern. A proportional-integral-derivative (PID) ILC with genetic algorithm was proposed by Lin, Wu e Hwang (2009); however the reference was a triangular signal. In (WU; ZOU; SU, 2009) and (WU; ZOU, 2009), an ILC was applied along side with a feedback controller in order to control the z axis of an AFM scanner.

1.1 Objectives

The main focus of this work is to propose a robust control strategy in order to track frequency varying sinusoidal signals. This dissertation applies the proposed control strategy in a numerical model of an atomic force microscope, where frequency-varying references may be used in order to improve scanning performances. The proposed methodology

makes use of a Frequency Varying Resonant Controller. In order to validate the proposed control system, the controller performance was compared to a traditional Proportional-Integral controller, and to a proposed Iterative Learning Control.

1.2 Manuscript Description

This dissertation is organized as follows. Chapter 2 describes the main background necessary for the comprehension of the proposed strategy. For example, it presents important information regarding: stability in the sense of Lyapunov concepts, which were subsequently applied in the control strategies defined by the robust control; Internal Model Principle and its application through the Resonant Control; Kalman Filter, used in order to estimated the system states necessary for the controller; and Atomic Force Microscopy area, such as functioning principles and operation difficulties. Chapter 3 will explain the Iterative Learning Control basic ideas and the design procedure for the spiral tracking, explaining how it relates with its application in a feedback closed-loop system. Then, Chapter 4 presents the main proposed control strategy, called Resonant Gain Scheduling Controller, which makes use of the previous information regarding the Lyapunov stability and robust control. This chapter is followed by Chapter 5 where the graphical and numerical results, obtained through simulations, are shown and discussed. Finally, Chapter 6 summarizes the main results presented in this dissertation, recalling the most important concepts and results found and presenting ideas for future works developments.

2 Background

In this chapter the main background concepts, used in the proposed control strategy, are presented. First, the concept of stability in the sense of Lyapunov is presented, being followed by the definition of Robust Control, a key element for the dissertation, using the Linear Matrix Inequalities approach. The chapter then explores the Internal Model Principle and the Resonant Control, the last being an important concept used in the proposed methodology in order to track sinusoidal signals. In the sequence, the Kalman Filter, used in order to achieve satisfactory state estimation, is revised. After, the Atomic Force Microscopy area is described, detailing its operation principles, applicabilities and limitations.

2.1 Stability in the Sense of Lyapunov

The stability in the sense of Lyapunov is a major theoretical development, for both linear and non-linear systems (KHALIL, 2002). It uses the concept of equilibrium points in order to determine the system stability. The first part of this section shows the basic definitions of stability in the sense of Lyapunov. In the second part, definitions regarding the stability of uncertain systems are presented.

2.1.1 Stability of discrete systems

Equilibrium point is an important concept for state equations. According to (KHALIL, 2002), a point $x = x^*$is said to be an equilibrium point of a system "if it has the property that whenever the state of the system starts at x^*, it will remain at x^* for all future time".

Consider the following autonomous system

$$x(k+1) = f(x(k)), \tag{2.1}$$

where $k \in \mathbb{Z}_+$ is the sample time, $x(k) \subseteq \mathbb{R}^n$ is the discrete system states vector in the sample time k and $f : \mathbb{R}_+ \times \mathbb{R}^n \to \mathbb{R}^n$ is the function that maps the states vector. For this autonomous system, the equilibrium points are the real roots of the equation $f(x(k)) = 0$.

Now, it is possible to define the main concepts regarding the stability of equilibrium points. This stability is evaluated using a function called Lyapunov function, i.e. $V(x(k))$.

Theorem 2.1. ***Stability of equilibrium points****: Let $x = 0$ be an equilibrium point for (2.1) and $\mathcal{D} \subset \mathbb{R}^n$ be a set containing $x = 0$. Let $V : \mathcal{D} \to \mathbb{R}$ be a continuous function in*

x such that:

$$\begin{aligned} V(x(0)) = 0 \quad \text{and} \quad & \Delta V(x(k)) < 0 \text{ in } \mathcal{D} - \{0\} \\ & \Delta V(x(k)) \leqslant 0, \quad \forall\, x \in \mathcal{D} \end{aligned} \tag{2.2}$$

- *Then, $x = 0$ is stable. Moreover, if*

$$\Delta V(x(k)) < 0, \quad \forall\, x \in \mathcal{D} - \{0\}. \tag{2.3}$$

- *then $x = 0$ is asymptotically stable.*

Now, let us consider the case of a discrete linear system in the form of

$$x(k+1) = Ax(k) \tag{2.4}$$

The stability condition for this type of system is given by the next Theorem.

Theorem 2.2. ***Stability in the sense of Lyapunov****: The system equilibrium point is asymptotically stable if there exists a symmetric positive matrix P such that*

$$A^\intercal PA - P < 0. \tag{2.5}$$

Proof. Let us consider the following quadratic Lyapunov function

$$V(x(k)) = x(k)^\intercal Px(k), \tag{2.6}$$

where P is a defined positive symmetric matrix with appropriate dimensions. The variation of $V(x(k))$ along the system trajectories is given by

$$\Delta V(x(k)) = x(k+1)^\intercal Px(k+1) - x(k)^\intercal Px(k). \tag{2.7}$$

Substituting (2.6) in (2.7)

$$\Delta V(x(k)) = x(k)^\intercal \left(A^\intercal PA - P\right) x(k). \tag{2.8}$$

If we assure that $P > 0$, then the first condition of the Theorem is satisfied. Furthermore, if $(A^\intercal PA - P) < 0$, then $\Delta V(x(k)) < 0$, which is a sufficient condition for the system stability. □

From now on, the notation "asymptotically stable system" will refers to the stability of the system origin.

2.1.2 Stability of discrete uncertain systems

An appropriate mathematical model of real systems may require the consideration of uncertainties. In these cases, it is necessary to specify the Lyapunov theory in order to address the system stability. Let us consider the following uncertain discrete system:

$$x(k+1) = A(\delta)x(k). \tag{2.9}$$

In order to address the uncertainty in the problem analysis, a possible approach is to define a polytope containing the maximum and minimum admissible values of any given uncertain parameter. Let us assume that $A(\delta)$ is an affine matrix on its uncertain parameters

$$A(\delta) = A_0 + A_1\delta \tag{2.10}$$

where δ is the uncertain parameter, which belongs to a closed set

$$\delta \in \left[\underline{\delta}, \quad \overline{\delta}\right], \tag{2.11}$$

where the extreme limits $\underline{\delta}$ and $\overline{\delta}$ are the lower and upper bounds of the parameter, respectively. When the dimension of δ is greater then one, they also describe a hyper-rectangle in $\mathbb{R}$, whose vertices are defined by

$$\upsilon \triangleq \left\{\lambda = (\lambda_1, \dots, \lambda_i) : \lambda_i \in \{\underline{\delta}, \overline{\delta}\}\right\} \tag{2.12}$$

From convexity arguments, it follows that if the inequalities conditions are satisfied in the polytope vertices, then the same restrictions will be satisfied inside the polytope (BERNUSSOU; PERES; GEROMEL, 1990). Therefore, it is possible to define the following theorem for systems with polytopic uncertainties:

Theorem 2.3. ***Stability in the sense of Lyapunov for polytopic uncertainties*** *(DUAN; YU, 2013)*[1]*: The system* (2.9) *is asymptotically stable, in the hyper-rectangle* υ*, if there is a symmetric positive matrix* $P \in \mathbb{R}^{n\times n}$ *such that*

$$A_i^{\intercal} P A_i - P < 0, \quad i = 1, \dots, h. \tag{2.13}$$

2.2 Robust Control

Robust control is a convenient method in order to solve control problems involving a system and its uncertainties. In this section, the main ideas regarding robust control are developed. First, robust state-feedback is defined, and then a performance requisite through pole placement is shown.

[1] The proof for this theorem can be found in the page 117 of (DUAN; YU, 2013).

2.2.1 Robust State-feedback

Besides the stability analysis, it is possible to make use of Lyapunov functions in order to design controllers. First, consider the following non-autonomous linear discrete system

$$x(k+1) = A(\delta)x(k) + B(\delta)u(k), \tag{2.14}$$

where $x(k) \in \mathbb{R}^n$ is the discrete states vector, $u(k) \in \mathbb{R}$ is the system input, and $A(\delta) \in \mathbb{R}^n$ and $B(\delta) \in \mathbb{R}^n$ are the system matrices that varies with the parameter δ.

A usual control strategy is the state-feedback, where the system states are multiplied by a fixed gain matrix $K \in \mathbb{R}^n$, as can be seen in the following control law:

$$u(k) = Kx(k). \tag{2.15}$$

If we consider uncertainties in the systems, it is possible to make use of the polytopic representation in order to obtain a robust state-feedback controller, that is, a controller that guarantees the stability of the system for any admissible value of the uncertaing parameters δ (BERNUSSOU; PERES; GEROMEL, 1990).

Theorem 2.4. ***State-feedback design for polytopic uncertainties****: Consider a system in the form of* (2.14) *and its polytopic representation in* (2.10)*. Suppose there exists a positive definite matrix $Q \in \mathbb{R}^{n\times n}$ and a matrix $Y \in \mathbb{R}^n$ such that the following LMIs are satisfied at the vertices of the polytope $\upsilon(\lambda)$*

$$\begin{bmatrix} Q & (A_iQ + B_iY)^\intercal \\ \star & Q \end{bmatrix} > 0, \quad i = 1, \ldots, h. \qquad Q > 0 \tag{2.16}$$

Then, system (2.9) *under control law* (2.15) *with $K = YQ^{-1}$ is asymptotically stable.*

Proof. Two conditions are necessary in order to demonstrate the proof. The condition $V(x(k)) > 0$ holds from the assumption that $P > 0$. For the second condition $\Delta V(x(k)) < 0$, consider

$$\begin{aligned} \Delta V(x(k)) &= V(x(k+1)) - V((x(k)) < 0 \\ &= x(k+1)^\intercal P x(k+1) - x(k)^\intercal P x(k) < 0 \end{aligned} \tag{2.17}$$

In closed loop, the system (2.9) takes the form of :

$$x(k+1) = (A(\delta) + B(\delta)K)x(k). \tag{2.18}$$

Substituting (2.18) in (2.17), we have

$$((A(\delta) + B(\delta)K)x(k))^\intercal P((A(\delta) + B(\delta)K)x(k)) - x(k)^\intercal P x(k) < 0,$$

which is equivalent to

$$(A(\delta) + B(\delta)K)^{\intercal}P(A(\delta) + B(^{\intercal}\delta)K) - P < 0. \tag{2.19}$$

According to Theorem 2.3, the inequality (2.13) is the same as in (2.19). Nevertheless, as (2.19) is a nonlinear expression, it requires some manipulation before being represented as an LMI. In order to make it linear, we may use the Schur complement, presented in the Definition 2.1.

Definition 2.1. Schur Complement: consider matrices $A \in \mathbb{R}^{n\times n}$, $B \in \mathbb{R}^{n\times m}$ and $C \in \mathbb{R}^{m\times m}$, such that $A = A^{\intercal}$, $C = C^{\intercal}$ and $C > 0$. According to Schur complement, the following expressions are equivalent

$$A - BC^{-1}B^{\intercal} > 0, \quad \begin{bmatrix} A & B \\ \star & C \end{bmatrix} > 0. \tag{2.20}$$

Applying the Schur complement in (2.19), we now have:

$$\begin{bmatrix} P & (A(\delta) + B(\delta)K)^{\intercal} \\ \star & P^{-1} \end{bmatrix} > 0, \quad P > 0 \tag{2.21}$$

Then, we may multiple both sides of (2.21) by a diagonal matrix

$$\begin{bmatrix} Q & 0 \\ 0 & I_{n\times n} \end{bmatrix}, \tag{2.22}$$

where $I \in \mathbb{R}^{n\times n}$ is a unit matrix and $Q = P^{-1}$, resulting in:

$$\begin{bmatrix} Q & QA(\delta)^{\intercal} + Y^{\intercal}B(\delta)^{\intercal} \\ \star & Q \end{bmatrix} > 0, \quad Q > 0 \tag{2.23}$$

where $Y = KQ$. Notice that (2.23) is equal to (2.16). Hence, the proof is complete. □

The uncertain systems definitions presented may also be applied to time-varying systems. The main difference between these two classes is that the second one has known functions that define how its parameters change over the time. Even if this approach may lead to conservative results in comparison, for example, to the parameter dependent Lyapunov functions (MONTAGNER; PERES, 2004), where the parameters variation may be considered in the problem, it is appealing due to its numerical simplicity, as it uses a simple Lyapunov function to determine a fixed gain in order to stabilize the uncertain system.

2.2.2 $\mathbb{D}$-stabilization

The previous controllers designs may not achieve a satisfactory performance if specific requisites are not taken into the problems. In this context, it is valueable to define a region of interest in the complex plane where one would like to place the poles of the closed loop system (DUAN; YU, 2013).

The $\mathbb{D}$-stabilization problem deals with the poles assignment of a system inside a specific region (BOYD, 1994). Using the LMIs property of multi objective optimization, the closed-loop poles can be placed using the controller design, through the addition of a constraint in the form of another LMI.

Let us consider that the LMI problem presented in (2.16) must define a feedback gain such that the control loop system poles are inside a disk with radius r and with center at coordinates c. In order to respect this restriction, it is possible to add the following LMI (DUAN; YU, 2013) to the optimization problem:

$$L \otimes Q + M \otimes (A_i Q + B_i Y) + M^{\intercal} \otimes (A_i Q + B_i Y)^{\intercal} < 0, \tag{2.24}$$

where $\otimes$ is the Kronecker product, and

$$L = \begin{bmatrix} -r & c \\ c & -r \end{bmatrix}, \qquad M = \begin{bmatrix} 1 & 0 \\ 0 & 0 \end{bmatrix} \tag{2.25}$$

By doing so, the calculated feedback gains will be able to lead the system poles to the specified region in the complex plane.

2.3 Internal Model Principle

The Internal Model Principle (IMP) is an adequate strategy for reference tracking and disturbance rejection (CHEN, 1999). According to (FRANCIS; WONHAM, 1976), if the model of the dynamics of the reference (or disturbance) signal is incorporated in the feedback path, it is possible to achieve asymptotic convergence of the tracking error. In this section, the IMP will be illustrated for a Single-Input Single-Output (SISO) system.

In order to explain the IMP functioning, consider the block diagram in the Figure 1, where: $R(s) \in \mathbb{C}$ is the reference signal, $E(s) \in \mathbb{C}$ is the error signal, $U(s) \in \mathbb{C}$ is the control signal, $C(s) = U(s)/E(s)$ is the controller transfer function, $Y(s) \in \mathbb{C}$ is the system output, and $G(s) = Y(s)/U(s)$ is the system transfer function.

It is possible to define the error $E(s)$ as a function of the reference.

$$\begin{aligned} E(s) &= R(s) - G(s)C(s)E(s) \\ &= \frac{1}{1 + G(s)C(s)} R(s). \end{aligned} \tag{2.26}$$

Figure 1 – Generic block diagram of a control system.

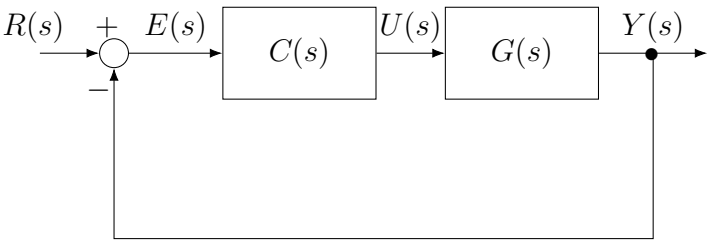

Expanding the following transfer functions to

$$R(s) = \frac{N_r(s)}{D_r(s)}, \quad C(s) = \frac{N_c(s)}{D_c(s)}, \quad G(s) = \frac{N_g(s)}{D_g(s)}, \tag{2.27}$$

and substituting in (2.26), with some algebraic manipulation:

$$E(s) = \frac{D_g(s)D_c(s)}{D_g(s)D_c(s) + N_g(s)N_c(s)} \frac{N_r(s)}{D_r(s)}. \tag{2.28}$$

Finally, considering the control block diagram defined in the Figure 1, the system error asymptotically tends to zero, i.e.

$$\lim_{t\to\infty} e(t) = 0,$$

where $e(t)$ is the inverse Laplace transform of $E(s)$, if and only if the following requirements are fulfilled (FRANCIS; WONHAM, 1976):

1. All closed-loop poles of $P_E(s) = D_g(s)D_c(s) + N_g(s)N_c(s)$ are in the left plane of the complex plane;
2. The polynomial $D_c(s)$ has all the marginally stable roots of the polynomial $D_r(s)$;
3. The polynomial $N_g(s)$ does not have any roots in common with $D_r(s)$.

Thus, the IMP controller can asymptotically tracks a signal by adding its dynamics into the closed-loop system.

2.3.1 Resonant Controller

In order to achieve better reference tracking, the present work proposes the application of the Internal Model Principle in the form of a resonant controller (WANG; CHU; TSAO, 2009). The resonant controller, in its simplest form, has the following structure:

$$C(s) = \frac{\omega_r^2}{s^2 + \omega_r^2}. \tag{2.29}$$

This controller introduces a valley in the frequency ω_r of the sensitivity function $S(j\omega) = E(j\omega)/R(j\omega)$, which relates the system error and the reference, as illustrate in

Figure 2 – Magnitude of Sensitivity Function Bode Diagram defined in (2.29), for $\omega_r = 100\,rad/s$ and an illustrative system $G(s) = 1/(s+10)$

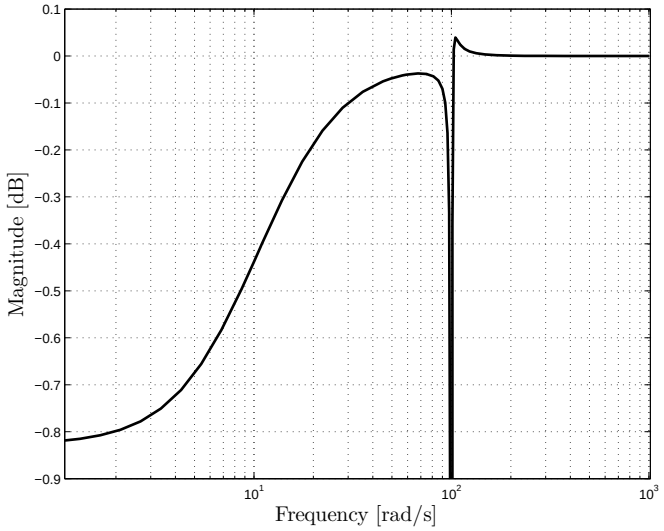

Figure 2. Thus, the gain of a sinusoidal reference with frequency ω_r for the system error is zero, which implies a perfect tracking.

Using the state-space notation, it is possible to rewrite the equation (2.29) as:

$$\begin{aligned} \dot{x}_r(t) &= A_r x_r(t) + B_r e(t) \\ y_r(t) &= C_r x_r(t) \end{aligned} \tag{2.30}$$

where $x_r \in \mathbb{R}^2$ is the resonant states vector, and $A_r \in \mathbb{R}^{2\times2}$, $B_r \in \mathbb{R}^{2\times1}$, $C_r \in \mathbb{R}^{1\times2}$ are defined as

$$A_r = \begin{bmatrix} 0 & \omega_r \\ -\omega_r & 0 \end{bmatrix}, B_r = \begin{bmatrix} 0 \\ 1 \end{bmatrix}, \quad C_r = \begin{bmatrix} 0 & \omega_r \end{bmatrix} \tag{2.31}$$

In order to use the continuous-time state space in the discrete framework, such as in a digital computer, a possible approach is to discretize the resonant system matrices using a convenient discretization technique (OGATA, 1987). For example, it is possible to cite the numerical integration methods Euler Forward, Euler Backwards and Tustin, the pole/zero matching method and the zero-order hold method. The sample time used in the discretization method must be faster than the system dynamics in order to generate an appropriate approximation of the original continuous representation (OGATA, 1987).

2.4 Kalman Filter

The seminal paper about the Kalman Filter (KF) was published in 1960, by Rudolph Emil Kalman (KALMAN, 1960). The KF is classified as a parametric Bayesian filter, allowing the recursive estimation of a dynamic system states in the presence of noise. It is possible to define an algorithm for the KF in two main steps (THRUN; BURGARD; FOX, 2005).

The first step is the prediction, where, using the mathematical model of the dynamic system, a prediction of the states values is performed for the sample k. The second step is the correction, where the states values measured by the sensors are used by the filter in order to correct the predictions of the first step. In the Kalman Filter, the system uncertain, represented by $\mathcal{R}$, and the sensors uncertain, represented by $\mathcal{Q}$, are parameterized in a Gaussian distribution form, which are composed by averages and covariances (THRUN; BURGARD; FOX, 2005). Besides the state observer function, the KF also performs a filtering in the measured signals, mitigating the presence of possible noises.

The Kalman Filter structure is describe in Algorithm 1 (THRUN; BURGARD; FOX, 2005), where the lines 2 and 3 refer to the prediction step, and the lines 4 to 6 refer to the correction step. The term Σ is the covariance of the states initial estimation. The term z refers to the output values measured by the sensors. Finally, the Kalman gain $\mathcal{K}$ is responsible for the weighting of the estimated and measured signals.

Algorithm 1 Kalman Filter Algorithm

1: KF $(u(k), z(k), x(k-1), \Sigma(k-1)$
2: $\quad \overline{x}(k) = A(k)x(k-1) + B(k)u(k)$
3: $\quad \overline{\Sigma}(k) = A(k)\Sigma(k-1)A(k)^{\intercal} + \mathcal{R}(k)$
4: $\quad \mathcal{K}(k) = \overline{\Sigma}(k)C(k)^{\intercal}(C(k)\overline{\Sigma}(k)C(k)^{\intercal} + \mathcal{Q}(k))^{-1}$
5: $\quad x(k) = \overline{x}(k) + \mathcal{K}(k)(z(k) - C(k)\overline{x}(k))$
6: $\quad \Sigma(k) = (I - \mathcal{K}(k)C(k))\overline{\Sigma}(k)$
7: Return $x(k), \Sigma(k)$

The previous algorithm considers that the system, represented in the state-space form, can be time-varying. If the working system has constant matrices, then it is possible to ignore the time dependency of the variables. Moreover, one may notice that if the system is time-invariant the Σ becomes a constant value, which reduces the filter computational cost.

2.5 Atomic Force Microscopy

The Atomic Force Microscopy (AFM) belongs to a larger group of instruments called Scanning Probe Microscopy (SPM), which started in 1982 with the invention of the Scanning Tunneling Microscope by Gerd Binnig and Heinrich Rohrer. According to Baró e Reifenberger (2012), the SPM instruments "are based on the strong distance-dependent interaction between a sharp probe or tip and a sample". These interactions can be, for example (TSUKRUK; SINGAMANENI, 2011): electrostatic, magnetic, chemical, conductive, among others physical phenomena.

In the AFM case, the basic concept is to measure the force between the tip (or probe) and the sample. The most common structure in this type of microscopes is to

mount the tip on the end of a cantilever, then either its dynamic properties change due to tip-sample forces or its static deflection can be used as measurement (MEYER; HUG; BENNEWITZ, 2004). Invented in 1986 by Gerd Binnin, Cal Quate and Christopher Gerber, the Atomic Force Microscope is very attractive to both industrial and academical researches (YABLON, 2014).

2.5.1 Operation Principles and Limitations

An Atomic Force Microscope operates using the measurement of forces between the sample surface and a sharp tip (TSUKRUK; SINGAMANENI, 2011). This nanometer tip is attached to the end of a cantilever, which is used as a transducer of the interaction. One method of amplifying and measuring this interaction is through the reflection of a laser beam with focus in the back side of the cantilever. A photodiode generates a voltage signal according to the position of the reflected laser beam. This signal is processed by a Digital Signal Processor (DSP), and then interpreted by a computer, which generates the scanning images.

Figure 3 – Atomic force microscope simplified schematic.

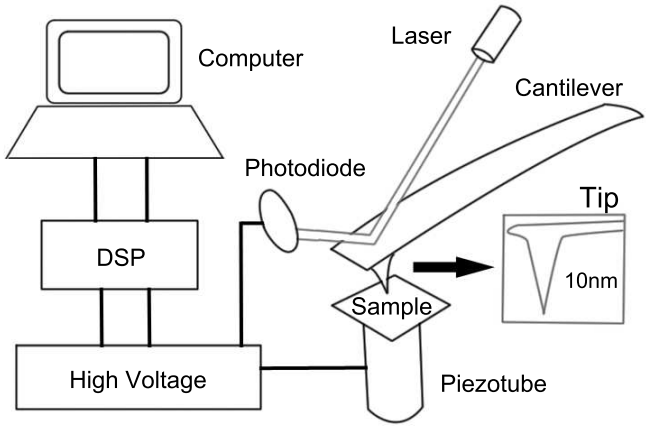

Based in (BARÓ; REIFENBERGER, 2012).

A simplified schematic of a common AFM scanner structure is depicted in Figure 3. Analysing the structure, it is possible to define four main components of the instrument (YABLON, 2014): the cantilever, the optical detection system (photodiode), the AFM software (DSP and computer) and the x-y-z scanner (piezotube and high voltage systems). These four main components will be detailed in the following.

The cantilever is the main part of the AFM, as it is responsible to provide the information of interest. According to Yablon (2014), the cantilever is typically made by a single-crystal of silicon (Si) or silicon nitride (Si_3N_4), and can be coated with gold and aluminium in order to obtain higher levels of reflectivity. The dimensions of the cantilever

are variable, and depend on the material to be scanned. The probe properties also depend on the application.

The optical detection system is responsible to track the cantilever as it performs the scanning. It consists in a position sensitive detector, normally a photodiode, that detects the reflection of a laser applied to the back side of the cantilever (BARÓ; REIFENBERGER, 2012). The AFM software is a critical part of the microscope, as it is responsible for controlling the motion of the x-y stage, the vertical distance between sample and probe, the subsequent data processing and image analysis.

Responsible for the microscope movements, the x-y-z scanner may operate either by considering a stationary tip or a stationary sample. Commercial instruments normally make use of piezoelectric materials in order to perform the necessary motions (MAROUFI; MOHEIMANI, 2016). The piezoelectric materials are able to contract or expand accordantly to an applied voltage, being capable to achieve motions in the magnitude of micron and even nanometers (YABLON, 2014). For example, the microelectromechanical systems (MEMS) nanopositioners are piezoelectric actuators that have reduced cost and higher bandwidths (MAROUFI; MOHEIMANI, 2016).

Two main movements must be executed by the scanner. The first one is the vertical movement in the z axis, responsible for the direct interaction between the tip and the sample surface. The second component is the x-y movement, responsible for the horizontal trajectory of the tip over the sample area. The x-y-z scanner may operate both in open-loop or closed-loop, according to the microscope structure (MEYER; HUG; BENNEWITZ, 2004).

The scanning pattern executed by the scanner tip, in the x-y plane, is a problem in particular. Most Atomic Force Microscopes operate using the raster scanning pattern (MAHMOOD; MOHEIMANI; BHIKKAJI, 2011), which can be seen in Figure 4. Its trajectory consists in a rectangular movement, being composed by a triangular signal in one axis, and a stair or ramp signal in the other axis. Atomic force microscopes commonly operate in open-loop in the x-y axes (MEYER; HUG; BENNEWITZ, 2004); otherwise, the closed-loop is mainly composed of PI controllers (ABRAMOVITCH et al., 2007; MAHMOOD; MOHEIMANI; BHIKKAJI, 2011).

Due to the presence of harmonics in the stair and the triangular signals, which difficult the control task, the raster pattern limits the scanning in higher velocities (RANA; POTA; PETERSEN, 2014). This fact may excite the instrument mechanical resonance frequency, and then create image deformations that can lead to possible scanning errors (MAHMOOD; MOHEIMANI; BHIKKAJI, 2011). In order to mitigate these difficulties, a possible solution is to substitute the raster scanning for more suitable patterns.

Some examples of patterns are: Cycloid (YONG; MOHEIMANI; PETERSEN,

Figure 4 – Examples of Scanning Pattern and its Cartesian components.

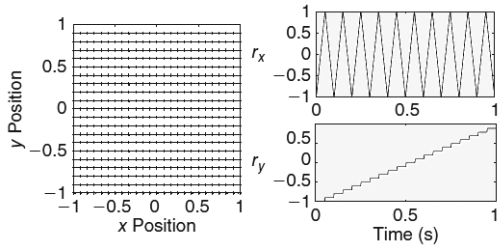

(a) Raster pattern.

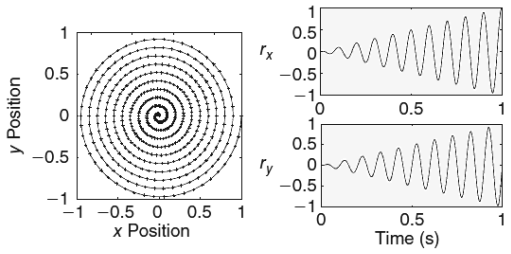

(b) Spiral pattern.

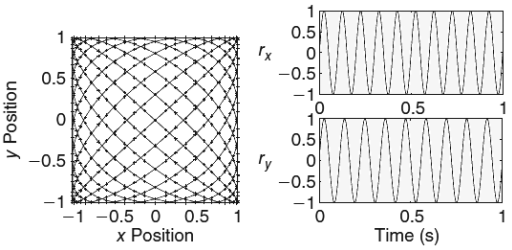

(c) Lissajous pattern.

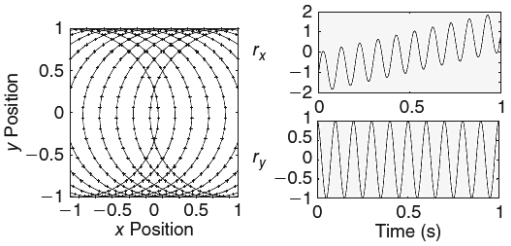

(d) Cycloid pattern.

Adapted from (TUMA et al., 2013).

2010), Lissajous (BAZAEI; YONG; MOHEIMANI, 2012) and Arquimedean Spiral (MAHMOOD; MOHEIMANI; BHIKKAJI, 2011). Four different examples of scanning patterns are presented in Figure 4: the traditional raster pattern, the spiral Archimedean pattern, the Lissajous pattern and the Cycloid pattern, along side with its respective Cartesian components.

2.5.2 Spiral Scanning Patterns

Among the different scanning patterns available in the AFM area, the Archimedean Spiral scanning pattern emerges as a good solution due to its unique properties (RANA; POTA; PETERSEN, 2014). Based in the homonym ancient geometric figure discovered by Archimedes in 3rd century BC, this pattern has constant distance between the M loops, i.e. pitch P. The spiral is composed by two different signals, applied to each of the scanner axes x and y. A frequency-varying spiral pattern and its respective signals are depicted in the Figure 5, where R_s is the spiral radius. The number of loops M is counted from the border to the center of the pattern.

The spiral is built from inside out, through the combination of two sinusoidal signals, applied to the horizontal plane axes of the AFM scanner. Using polar coordinates, it is possible to define the radius r and the angle θ, used to obtain the sinusoidal signal, as (ZIEGLER et al., 2017):

$$\begin{aligned} r &\triangleq R_s f(t_*) \\ \theta &\triangleq 2\pi M f(t_*), \end{aligned} \tag{2.32}$$

Figure 5 – Archimedean frequency-varying spiral pattern with $R_s = 1\mu$m, $M = 5$ and $P = 2 \times 10^{-7}$, and its respective x and y axes components.

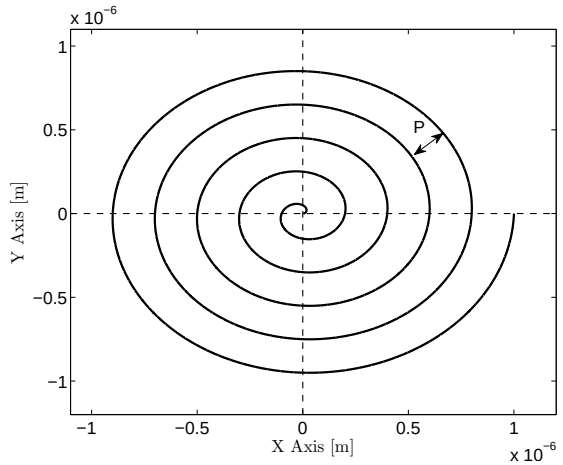

(a) Archimedean spiral pattern with $R_s = 1\mu$m, $M = 5$ and $P = 2 \times 10^{-7}$.

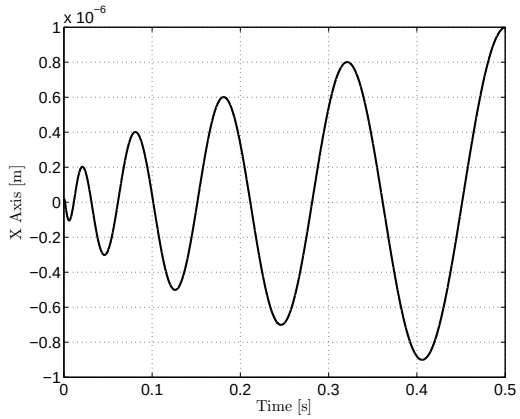

(b) Archimedean spiral pattern x axis.

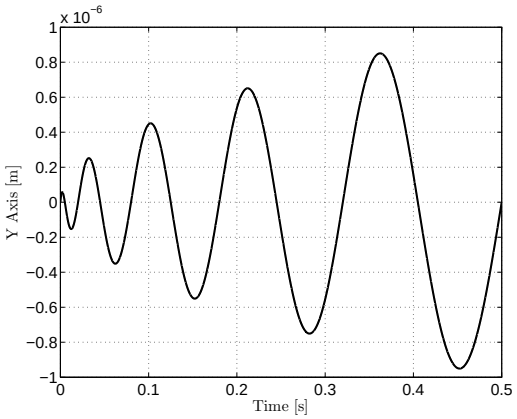

(c) Archimedean spiral pattern y axis.

where $f(t_*)$ is a function that determinate the spiral properties, R_s is the spiral radius and M is the pattern number of loops. The term t_* is a normalized time variable, that considers $t_* = t/T$, where t is the time, and T is the required time to complete the scan pattern.

The scanner tip linear velocity v and angular velocity ω are given by

$$\begin{aligned} v &\triangleq \frac{R_s f'(t_*)}{T}\sqrt{(2\pi M f(t_*))^2 + 1} \\ \omega &\triangleq \frac{2\pi M}{T} f'(t_*) \end{aligned} \tag{2.33}$$

where $f'(t_*)$ denotes the derivative of $f(t_*)$ with respect to the normalized time t_*.

The Archimedean Spiral can be generated using two basic different methods. It is possible to consider a trajectory with a constant angular velocity (CAV) or a constant linear velocity (CLV) (MAHMOOD; MOHEIMANI, 2010). Both methods have specific implications in the scanning performance.

2.5.2.1 CAV spiral

The CAV pattern considers the angular velocity a constant parameter, varying the linear velocity with the curves radius. The CAV function is defined as (ZIEGLER et al., 2017)

$$f(t_*) = t_*. \tag{2.34}$$

Substituting 2.34 in 2.33, we obtain the CAV linear velocity v_a and angular velocity ω_a:

$$\begin{aligned} v_a &= \frac{R_s}{T}\sqrt{(2\pi M t_*)^2 + 1}, \\ \omega_a &= \frac{2\pi M}{T}. \end{aligned} \tag{2.35}$$

It is clear from the above that the angular velocity is a constant value. This fact results in small linear velocities in the center and large linear velocities in the periphery, which may lead to under sampling (ZIEGLER et al., 2017).

2.5.2.2 CLV spiral

In the CLV pattern, the linear velocity is considered a constant parameter. Therefore, the angular velocity varies according to the curves radii. The CLV function is defined as (ZIEGLER et al., 2017)

$$f(t_*) = \sqrt{t_*}. \tag{2.36}$$

Substituting (2.36) in (2.33), the CLV linear velocity v_l and angular velocity ω_l can be obtained by:

$$\begin{aligned} v_l &= \frac{R_s\sqrt{(2\pi M)^2 t_* + 1}}{2T\sqrt{t_*}} \\ \omega_l &= \frac{\pi M}{T\sqrt{t_*}}. \end{aligned} \tag{2.37}$$

When $t_* \gg 1/(2\pi M)^2$, the linear velocity approaches a constant value $v_l = \pi M R_s/T$. Nevertheless, toward the very beginning of the CLV spiral, the angular velocity value (and the linear velocity, as well), theoretically, approach infinity. This fact leads to poor sampling in the center of the spiral scan (ZIEGLER et al., 2017).

2.5.2.3 Optimal Archimedean Spiral

Aiming to mitigate the disadvantages of both cases, a composed pattern, called Optimal Archimedean Spiral (OPT), was proposed by Ziegler et al. (2017). The spiral optimal parameterization is done such that the scan time is the least possible respecting the linear and angular velocity constraints of the microscope. It consists in a switched

trajectory: in the center of the pattern, the OPT follows a constant angular value ω_o, and in the periphery, it follows a constant linear velocity v_o.

The moment for the transition is defined as the normalized instant t_{*o}. When the spiral reaches t_{*o}, the angular velocity ω_o corresponds to a linear velocity v_o value such that the transition is smooth, and the radius does not suffer any abrupt variation. The OPT spiral function $f(t_*)$ of the normalized time t_* is defined by:

$$f(t_*) = \begin{cases} \frac{t_*}{a}, & \text{if} \quad t_* \leqslant t_{*o} \\ \sqrt{c_1 t_* + c_2}, & \text{if} \quad t_* > t_{*o}, \end{cases} \tag{2.38}$$

where

$$\begin{aligned} a &\triangleq \frac{2\pi M}{T\omega_o}, \\ c_1 &\triangleq \frac{2t_*}{a^2}, \\ c_2 &\triangleq 1 - c_1. \end{aligned} \tag{2.39}$$

Therefore, the OPT pattern follows a variable linear velocity in the beginning of the trajectory, and a variable angular velocity in its end (for $t_* > t_{*o}$). The reference for each axis is given by the relation between polar and Cartesian coordinates:

$$\begin{aligned} r_{\mathrm{x}} &= r\cos(\theta), \\ r_{\mathrm{y}} &= r\mathrm{sen}(\theta), \end{aligned} \tag{2.40}$$

where $r \triangleq R_s f(t_*)$, $\theta \triangleq 2\pi M f(t_*)$, and r_{x} and r_{y} are the reference signal for the x and y axes, respectively.

By doing so, the OPT is able to take advantage of the benefits of both methods. From the beginning, the OPT linear velocity increases, as the angular velocity is constant. When the time t_* reaches the transition instant t_{*o}, the OPT switches its function to a constant linear velocity. Then, the angular velocity decreases proportionally, until the spiral is complete. The switch does not create an abrupt change in the spiral frequencies values, which is important for the proposed control method of the present work.

According to Ziegler et al. (2017), besides the velocity issues, the OPT pattern has many advantages over other patterns, such as highly homogeneous sampling and small information discard over the scanning image. Despite the advantages of the presented OPT spiral, the only known work that proposed a controller in order to track it was found in (BAZAEI; MAROUFI; MOHEIMANI, 2017).

2.6 Final Considerations

This chapter presented the main background information that will be used by the remaining of the dissertation. First, the stability in the sense of Lyapunov was developed,

including the system with uncertainty approach. In the sequence, the concepts of robust control were introduced, being followed by the Internal Model Principle definitions and its application through the Resonant Control. In the sequence, the Kalman Filter, used to estimated the system states, was reviewed. Finally, the main information regarding the AFM was presented, including its operation principles and limitations, where the application of spiral references as an option to improve the scanning performance was detailed, along side with its implementation difficulties.

3 Iterative Learning Control for Spiral Tracking

This chapter presents the main information regarding the Iterative Learning Control strategy. First, the basic ideas about the ILC are presented. It includes the ILC functioning principles, detailing how the controller can makes use of past batches informations in order to improve the system general performance, main definitions regarding theorems and how the controller can be properly implemented. In the sequence, a procedure design for the Iterative Learning Control, based in how the ILC is related to a system already controlled by a feedback loop, is detailed for the spiral reference tracking.

3.1 Basic Results on Iterative Learning Control

Iterative Learning Control is an area of the control theory that has attracted a great popularity over the past years (OWENS, 2015). One of the first academic works about ILC was published in 1978 in Japan, and it became an active research area after 1984 (NORRLOF; GUNNARSSON, 2002). The ILC functioning principle is based on the notion that tasks performed multiple times can be better executed if the system learns from its previous executions. Using the information of previous batches, the controller may use a specific logic in order to reduce the error from the last iteration. After a determinate number of batches, the error will converge to zero or to a small acceptable value.

In order to further develop the ILC concepts, it is necessary to state the definition of iteration. One iteration is a complete batch, composed by N samples. Each time a new iteration begins, the batch starts again from the sample time $k = 1$ to the last sample N. In order to clearly define the difference between sample and iteration, let us consider the variable $c_j(k)$. The subscript j refers to the iteration and k refers to the sample. For example, $c_1(2)$ is the variable c value in sample time 2 on the first iteration. It is important to notice that the ILC starts operating always from the second iteration, as its algorithm needs the previous information in order to affect the system.

Now we proceed to the formal concepts about this control strategy. For the ILC concepts in this section, the system will be represented using the so called lifted form, as follows (BRISTOW; THARAYIL; ALLEYNE, 2006):

$$\mathbf{y}_j = \mathbf{G}\mathbf{u}_j + \mathbf{d}, \tag{3.1}$$

where

$$\begin{bmatrix} y_j(1) \\ y_j(2) \\ \vdots \\ y_j(N) \end{bmatrix} = \begin{bmatrix} g[1](0) & 0 & \dots & 0 \\ g[2](1) & g[1](1) & \dots & 0 \\ \vdots & \vdots & \ddots & \vdots \\ g[N](N-1) & g[N-1](N-1) & \dots & g[1](N-1) \end{bmatrix} \begin{bmatrix} u_j(0) \\ u_j(1) \\ \vdots \\ u_j(N-1) \end{bmatrix} + \begin{bmatrix} d(1) \\ d(2) \\ \vdots \\ d(N) \end{bmatrix}, \tag{3.2}$$

The output $\mathbf{y}_j \in \mathbb{R}^N$ is related with the input $\mathbf{u}_j \in \mathbb{R}^N$ through the unit-pulse response matrix $\mathbf{G} \in \mathbb{R}^{N \times N}$, whose coefficients are given by the system unit-pulse response at each sample k during all the length of each batch N. The term $\mathbf{d} \in \mathbb{R}^N$ represents an exogenous signal, such as noise or disturbances. Note that this notation allows the system to be time-varying; otherwise, if the system was time-invariant, then the coefficients $g[1], g[2], ..., g[N-1]$ would not change over time. It will be assumed hereafter that the system is stable.

It is possible to obtain the lifted form from the traditional state-space form of a linear time-varying system

$$\begin{aligned} x(k+1) =& A(k)x(k) + B(k)u(k) \\ y(k) =& C(k)x(k) + D(k)u(k) \end{aligned} \tag{3.3}$$

where $x \in \mathbb{R}^n$ is the state vector, $u(k) \in \mathbb{R}$ is the control input, and A, B, C and D are definite and have appropriate dimensions, through the following relation:

$$g_i(k) = \begin{cases} D(k), & \text{if } i = 1 \\ C(k)A^{i-1}(k)B(k), & \text{if } N-1 \geqslant i > 1 \end{cases} \tag{3.4}$$

As the ILC is a control strategy, there are many different ways in order to apply it. Its structure may include filters, proportional, integral and derivative gains, among other options. The present work will make use of a well-known ILC algorithm, defined as follows (OWENS, 2015):

$$\mathbf{u}_{j+1} = \mathbf{Q}(\mathbf{u}_j + \mathbf{L}\mathbf{e}_j), \tag{3.5}$$

where $\mathbf{u}_j \in \mathbb{R}^n$ is the ILC control input vector in the j-th iteration, $\mathbf{Q} \in \mathbb{R}^{N \times N}$ is the Q-Filter, $\mathbf{L} \in \mathbb{R}^{N \times N}$ is the learning function, $\mathbf{e}_j = \mathbf{r} - \mathbf{y}_j$ is the error vector obtained from the reference trajectory vector $r \in \mathbb{R}^n$, which is considered invariant iterations, i.e. the same sequence for every iteration, and the output vector y_j. Both $\mathbf{Q}$ and $\mathbf{L}$ are matrices that can be obtained from their state-space representation in the same way that the lifted system using the relation (3.4).

The learning function and the Q-Filter are responsible to weight the effect of the previous values of the error and the control input, respectively, in the current control input. Both of them may assume different forms: low-pass filters, band-pass filters, constant gains (BRISTOW; THARAYIL; ALLEYNE, 2006). Moreover, their design may also

be performed in different ways, from quadratic performance criterion to plant dynamics inversion.

Figure 6 shows how the ILC controller, detached by the dotted square, is added in a classic feedback loop. The *Memory* blocks are responsible to save the information about each iteration, in order to use them in the next execution. Note that the control input u is composed by the feedback controller C signal, u_{FB}, and the ILC controller signal, u_{ILC}.

Figure 6 – Iterative Learning Control block diagram. The final control input u is the summation of the feedback and the ILC controller outputs u_{FB} and u_{ILC}, respectively.

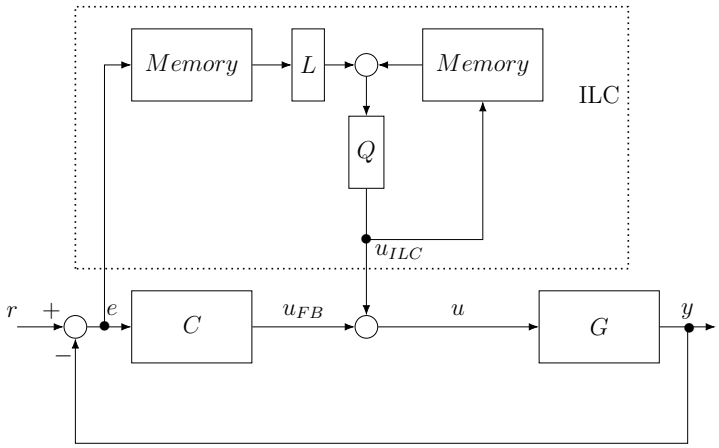

3.1.1 Stability Conditions

In order to define the concepts of stability for a system controlled by ILC, it is necessary to introduce some convenient postulates (NORRLOF; GUNNARSSON, 2002). They are important for the theorems that follow and also to define the basic concepts of the ILC algorithm. The six postulates are listed as follows:

1. Every iteration has a fixed duration time N;
2. The reference $r(k)$ is given *a priori* over all the duration time $k \in [0, N]$;
3. The initial conditions are the same for each iteration. This means that, considering a state-space representation, $x_j(0) = x_0(0), \quad j = 0, 1, 2, ...$
4. The system dynamics do not change over the iterations;
5. It is possible to measure the output in every sample in order to calculate the respective error;
6. Given a reference $r(k)$, with a piecewise continuous derivative, there exists a unique input $u_d(k)$ such that the output is equal to $r(k)$.

Another important definition for the stability concepts using ILC is the ϵ-convergence (NORRLOF; GUNNARSSON, 2002), which assumes that the sixth postulate is true.

Definition 3.1. (ϵ-convergence): a system using ILC is ϵ-convergent in a norm $||\cdot||$ if

$$\limsup_{j\to\infty} ||u_d - u_j|| < \epsilon, \tag{3.6}$$

for some $\epsilon < \infty$.

It is important to note that stability does not imply a smaller error from one iteration to the next. For the next concept, let us introduce a generic *linear iterative system*

$$\mathbf{i}_{j+1} = \mathbf{H}\mathbf{i}_j + \mathbf{P}\mathbf{p}, \tag{3.7}$$

where $\mathbf{i} \in \mathbb{R}^N$, $\mathbf{p} \in \mathbb{R}^N$, $\mathbf{H} \in \mathbb{R}^{N\times N}$ and $\mathbf{P} \in \mathbb{R}^{N\times N}$.

Now an important property of this class of system, the BIBO stability, is defined.

Definition 3.2. BIBO stability of a linear iterative system: A linear iterative system is BIBO stable if a bounded input, $||\mathbf{p}|| < \infty$, generates a bounded output, $||\mathbf{i}_j|| < \infty$, for all j.

Using this class of system and this definition, we may now define the first Theorem regarding the stability of ILC.

Theorem 3.1. ***BIBO stability of a linear iterative system****: A linear iterative system*

$$\mathbf{i}_{j+1} = \mathbf{H}\mathbf{i}_j + \mathbf{P}\mathbf{p} \tag{3.8}$$

is BIBO stable if

$$\rho\left(H < 1\right), \tag{3.9}$$

where $\rho(M) = \max_{i=1,\ldots,n} |\lambda_i(M)|$*, and* $\lambda_i(M)$ *is the i-th eigenvalue of the matrix* $M \in \mathbb{R}^{n\times n}$*.*

Proof. Given the iterative system structure described in (3.7), one may note that it is the same as the traditional discrete-time systems (OWENS, 2015)[1], where asymptotic stability of $x(k+1) = Ax(k)$ is equivalent to the eigenvalues of the system being inside the unitary disc, i.e. $\rho\left(H < 1\right)$ (CHEN, 1999). □

Using the previous concepts, it is possible to define the following Theorem for the stability of a system controlled by ILC algorithm.

[1] Note that an iteration system and a discrete-time system are similar as both consist of a vector of states depending on its previous values and a determinate input.

Theorem 3.2. ***Stability of a system controlled by ILC****: A system in the form of* (3.1)*, controlled by the ILC algorithm as in* (3.5)*, is stable if*

$$\rho\left(Q(I_{N\times N} - LG)\right) < 1. \tag{3.10}$$

Proof. First, let us consider the algorithm (3.5). If we substitute (3.1) in (3.5):

$$\begin{aligned} \mathbf{u}_{j+1} =& Q(\mathbf{u}_j + L(\mathbf{r} - \mathbf{y})) \\ =& Q(\mathbf{u}_j + L\mathbf{r} - LG\mathbf{u} - LG\mathbf{d})) \\ \mathbf{u}_{j+1} =& Q(I - LG)\mathbf{u}_j + QL(\mathbf{r} - \mathbf{d}) \end{aligned} \tag{3.11}$$

Considering that the ILC algorithm is ϵ-convergent, according to the Definition 3.1, and that the last equation is in the same form of an iterative learning system from the Theorem 3.1, then the controlled system is stable if $\rho\left(Q(I - LG)\right) < 1$.

□

3.2 Iterative Learning Control Procedure Design

Using the basic concepts previously developed, this section will present the procedures used in order to properly design the controller learning function and Q-Filter. In order to further develop this chapter, consider the following closed-loop system depicted in Figure 7.

Figure 7 – Closed-loop system for the first iteration.

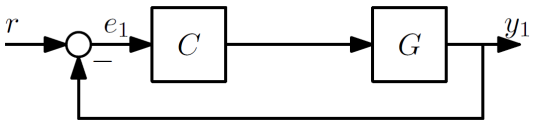

The discrete feedback controller $C(z)$ is responsible to stabilize the discrete system $G(z)$. In this structure, the sensitivity function is defined as $S(z) = (1 + G(z)C(z))^{-1}$. Recalling the definition of iteration, which consists in a complete batch of the system, the error e_1 is given by the sensitivity function and the reference signal r, of size N, given by $e_1(z) = S(z)r$. While the controller may stabilize the system, the iteration may end with a significant remaining error. And it is in this situation where the Iterative Learning Control can show its potential.

Now let us consider that the system must repeat the reference tracking several times. In this second iteration, the reference signal r is the same applied to the first one. According to the ILC main concept, it is possible to make use of the past error value in order to improve the controller performance. In other words, the information regarding the previous task can be applied in the current one.

Figure 8 represents this concept of using the previous error information in the current iteration. The new batch structure is the same as the last one, with the exception that the control input generated by the feedback controller is summed with the signal f_2, which is the first iteration error e_1 mapped by the learning filter $L(z)$.

Figure 8 – Closed-loop system for the second iteration.

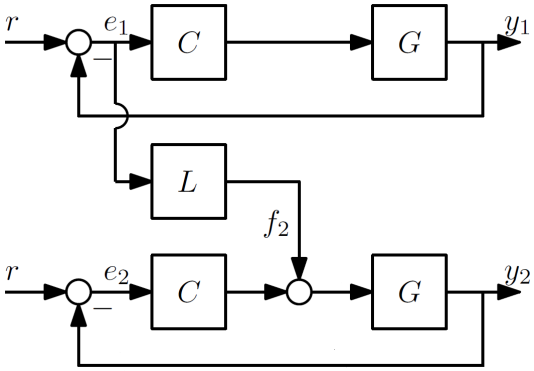

While the first iteration error was computed directly by the subtraction of the reference and the output signal, in the second iteration the error e_2 is given by $e_2(z) = S(z)r - S(z)G(z)f_2$. As the signal f_2 is defined as $f_2(z) = L(z)e_1$, we may now define the second batch error as $e_2(z) = S(z)r - S(z)G(z)L(z)e_1$. The question now is how to design $L(z)$ such that the error can be eliminated or reduced.

Analysing the e_2 equation, one may note that if the learning function is defined as $L(z) = (S(z)G(z))^{-1}$, the error converges to zero, i.e. $e_2 = 0$. Although this solution may look straightforward, there are situations where the direct inversion may not guarantee the error equal to zero. For example, if there are uncertainties in the models, some dynamics may not be fully compensated by the learning function. Another situation is if the transfer functions has non-minimum phase zeros or unstable poles, which would lead to an unstable behavior of the learning function.

Even if the direct cancellation of the functions is not possible, the Iterative Learning Control main idea of using the last tasks information can be continuously applied in the next batches. While it may not result in an error equal to zero, it can generate better performance levels over the execution of the system tasks. Figure 9 represents how the third iteration can be represented: the system output y_3 now depends on the feedback controller and on the two previously performed iteration.

It is possible to see that the next iteration error can be obtained from the previous one through the relation $e_{j+1} = (1 - G(z)S(z)L(z))e_j$ (BOEREN et al., 2016). Therefore, the ILC controller stability would involve the analysis of the relation $(1 - G(z)S(z)L(z))$ (BRISTOW; THARAYIL; ALLEYNE, 2006). Nevertheless, it is well-know in the ILC theory that most applications require a Q-Filter $Q(z)$ in order to achieve a satisfactory

Figure 9 – Closed-loop system for the third iteration.

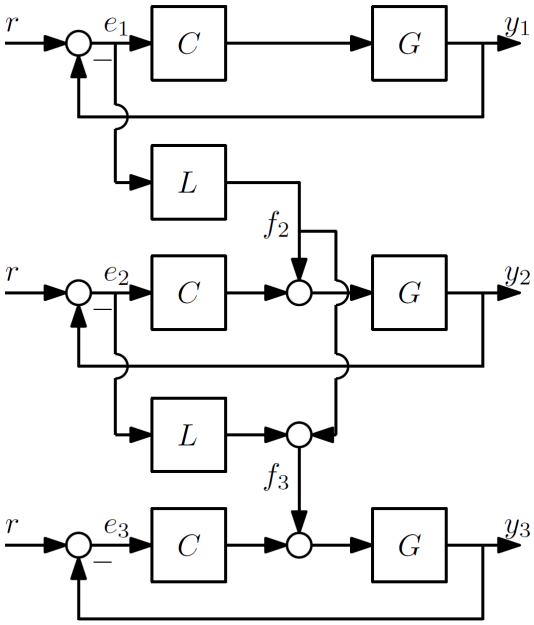

tradeoff between stability and performance (BRISTOW; THARAYIL; ALLEYNE, 2006). The Q-Filter is responsible for filtering the control signal generated by the ILC controller, as presented in Figure 6. So, the stability condition must consider the relation $Q(z)(1 - G(z)S(z)L(z))$ (WU; ZOU, 2009).

A sufficient condition for the controller stability, similar to the one presented in the basic ILC definition in the Background chapter, can be defined now for the frequency domain.

Theorem 3.3. ***ILC stability in frequency domain*** *(BOEREN et al., 2016)*[2]*: The two-norm of the ILC control input, generated in a closed loop with a discrete system $G(e^{jw})$, controlled by both a feedback $C(e^{jw})$ and an ILC, composed by a Q-Filter $Q(e^{jw})$ and a learning function $L(e^{jw})$ as presented in 6, controllers, will converge if*

$$|Q(e^{jw})(1 - G(e^{jw})S(e^{jw})L(e^{jw}))| < 1, \tag{3.12}$$

where $S(e^{jw}) = (1 + C(e^{jw})G(e^{jw}))^{-1}$ is the sensitivity function and the two-norm $||.||$ of a vector $v \begin{bmatrix} v_1 & v_2 & \dots & v_n \end{bmatrix}$ is computed by $||v|| = \sqrt{v_1^2 + v_2^2 + \dots + v_n^2}$.

Another important point for the Iterative Learning Control design and implementation is the structures of both the $L(z)$ and $Q(z)$ filters. As state before, a possible procedure to design the learning function is to make it $L(z) = (S(z)G(z))^{-1}$ and then use the Q-Filter to enforce robustness in the ILC structure, in order to achieve the condition $|Q(e^{jw})((1 - G(e^{jw})S(e^{jw})L(e^{jw}))| < 1$. Nevertheless, both the learning function and the

[2] The proof for this theorem can be found in the respective reference.

Q-Filter discrete transfer functions must respect other two conditions in order to be able to be applied as filters in the input and error signals.

These conditions are that both discrete functions must be stable, i.e. eigenvalues with module less than 1, and causal, i.e. the filter does not depends on future values of the output (CHEN, 1999). If the filter transfer function is not causal, then it is possible to add fast poles into its denominator. By doing so, the system will respect the causality property and will not be significantly affected by the artificial poles.

According to the previously presented information, it is possible to resume the ILC design procedure into two main steps, defined as follows.

1. Design the learning function $L(z)$ in order to cancel the stable poles and zeros of the system $G(z)$, i.e. make $L(z) = (1 + G(z)C(z))^{-1}$, where $C(z)$ is the feedback controller and $S(z)$ is the sensitivity function;

2. Design the Q-Filter $Q(z)$ to satisfy (3.12) without compromising the system bandwidth, in order to achieve a satisfactory tradeoff between performance and stability.

3.3 Final Considerations

In this chapter, the Iterative Learning Control was explained, including its main concepts, stability definitions and application structures. In the sequence, a procedure design for the spiral reference signal was detailed. The procedure was based in the ILC relation with a system already controlled by a feedback controller: the residual error obtained during each task can be used in the next iteration, in order to improve the general performance. The error is mapped in the next batch through the learning function, which can be designed such that the system dynamics can be compensated. In order to enforce robustness, the Q-Filter can be also used in the ILC structure.

4 Resonant Gain Scheduling Controller

This chapter presents the main contribution of this dissertation: the Resonant Gain Scheduling Controller. This controller combines the previously shown concepts, and this section details the procedures used to design and implement the controller. It is divided in three main parts. The first one presents the augmented system, using the resonant controller, and the polytopic representation. The second part explains the resonant gain scheduling controller design procedure using an optimization problem, that makes use of the augmented and polytopic representation and also the $\mathbb{D}$-stabilization. The third part presents the final structure of the controller diagram, depicting how the resonant system and the feedback gains are organized. The diagram also shows how the other parts of the work, such as the Kalman Filter and the Iterative Learning Control, are integrated to the closed-loop structure.

4.1 Augmented System and Polytopic Representation

As presented in the Background chapter, the Internal Model Principle may be used in order to achieve satisfactory reference tracking. In the present work, the reference signals have sinusoidal dynamics, which allows the application of the IMP through the Resonant Control.

A possible approach to integrate the RC dynamics into the closed-loop path is to define an augmented structure, using the system state-space matrices. By doing so, the controller gains can be designed such that the resonant system is also considered and then the reference can be adequately tracked. First, let us consider the following discrete state-space system:

$$\begin{aligned} x(k+1) &= Ax(k) + Bu(k) \\ y(k) &= Cx(k) + Du(k) \end{aligned} \tag{4.1}$$

where $x \in \mathbb{R}^n$ is the system states vector, $u \in \mathbb{R}$ is the control input, $y \in \mathbb{R}$ is the system output, $A \in \mathbb{R}^{n \times n}$, $B \in \mathbb{R}^n$, $C \in \mathbb{R}^{1 \times n}$ and $D \in \mathbb{R}$.

Using the system matrices, it is possible to define an augmented system making use of the resonant system matrices, presented in the Background chapter. The augmented system is given by:

$$\begin{aligned} x_a(k+1) &= A_a x_a(k) + B_a u(k) \\ y(k) &= C_a x_a(k) + D_a u(k) \end{aligned} \tag{4.2}$$

where $x_a(k) = \begin{bmatrix} x(k) & x_r(k) \end{bmatrix}^\top$ is the augmented system state vector, which is composed by the discrete system state vector $x(k)$ and the discrete resonant state vector $x_r(k)$. The augmented system matrices are defined as follows:

$$\begin{aligned} A_a(k) &= \begin{bmatrix} A & 0 \\ -C & Ad_r(k) \end{bmatrix} \qquad B_a(k) = \begin{bmatrix} B \\ Bd_r(k)D \end{bmatrix} \\ C_a &= \begin{bmatrix} C & 0_{1\times 2} \end{bmatrix} \qquad\qquad D_a = D. \end{aligned} \tag{4.3}$$

where $Ad_r(k)$ and $Bd_r(k)$ are the discrete representation of the resonant matrices $A_r(k)$ and $B_r(k)$, defined in the Section 2.3.1. The matrices can be discretized using a convenient discretization method and are replicated here for the convenience of the reader:

$$A_r = \begin{bmatrix} 0 & \omega_r \\ -\omega_r & 0 \end{bmatrix}, B_r = \begin{bmatrix} 0 \\ 1 \end{bmatrix}, \quad C_r = \begin{bmatrix} 0 & \omega_r \end{bmatrix} \tag{4.4}$$

As it is possible to see in (4.3), that the augmented system depends on the variation of the resonant controller, which is defined according to the spiral reference frequency-varying signal described in Background section. The frequencies values, obtained from the spiral patterns definitions, belongs to a known range

$$\omega \in \begin{bmatrix} \underline{\omega}, & \overline{\omega} \end{bmatrix}, \tag{4.5}$$

where the extreme limits $\underline{\omega}$ and $\overline{\omega}$ are the frequency lower and upper bounds, respectively. These bounds will be used in order to define the range for the controller design in the next section. They also describe a convex space in $\mathbb{R}$, whose vertices are defined by

$$\upsilon \triangleq \{\omega = (\omega_1, \dots, \omega_j) : \omega_i \in \{\underline{\omega}, \overline{\omega}\}\} \tag{4.6}$$

Considering that the frequency values for the resonant matrices are limited by the two bounds defined in (4.5), it is possible to define two bounds for the augmented system matrices that depend on the frequency values. These two different augmented matrices A_a and B_a are defined using the structure in (4.3) and the limits defined in the polytope (4.5).

In the lower limit, or when $\omega = \underline{\omega}$, the augmented matrices are defined as $\underline{A_a}$ and $\underline{B_a}$. On the other hand, in the higher limit, when $\omega = \overline{\omega}$, the augmented matrices are defined as $\overline{A_a}$ and $\overline{B_a}$. These two matrices sets will be used for the controller design presented in the following section.

4.2 Gain Scheduling via Linear Matrix Inequalities

Using the previously defined augmented matrices, constructed using the polytopes describing the lower and the higher bounds of the resonant system frequencies, the feedback gains of the controller can be computed through the Lyapunov stability approach

organized using LMIs in an optimization problem. The proposed control law takes the form of a gain scheduling controller, and is defined as:

Definition 4.1. Gain Scheduling controller (BOYD, 1994): a state-feedback controller whose parameters can depend on the system parameters.

In the present work, the controller is function of the parameter ω, recalling that ω is the reference signal frequency value, obtained from the sinusoidal signals define by the equations presented in Section 2.5. Therefore, the resonant gain scheduling control law is defined as follows:

$$u(k) = (K_0 + K_1\omega)x_a(k), \tag{4.7}$$

where $K_0 \in \mathbb{R}^n = \begin{bmatrix} K_{0x} & K_{0r} \end{bmatrix}$ and $K_1 \in \mathbb{R}^n = \begin{bmatrix} K_{1x} & K_{1r} \end{bmatrix}$ are the augmented feedback gain vectors, composed by the system gains K_{0x} and K_{1x}, and the resonant gains K_{0r} and K_{1r}.

Making use of the control law (4.7) and the augmented matrices defined in the frequency bounds (4.5), it is possible now to define a Theorem for the calculation of the resonant gain scheduling feedback gains. This Theorem makes use of the polytopic representation, and the control design becomes an optimization problem subject to constraints in the form of Linear Matrix Inequalities. From convexity arguments, by assuring the stability of the system for the maximum and minimum values of ω, one achieves the stability for any $\omega \in \begin{bmatrix} \underline{\omega}, & \overline{\omega} \end{bmatrix}$.

Theorem 4.1. *Consider an augmented system in the form of* (4.2) *and its polytopic representation* (4.5)*. Suppose there exists a positive definite matrix* $Q \in \mathbb{R}^{n\times n}$ *and a matrix* $Y \in \mathbb{R}^{n\times n}$ *such that following LMIs are satisfied at the vertices of the polytope* (4.6)

$$\begin{aligned}
\begin{bmatrix} Q & (\underline{A_a}Q + \underline{B_a}Y_0 + \underline{B_a}Y_1\omega_{min})^\intercal \\ \star & Q \end{bmatrix} > 0, \\
\begin{bmatrix} Q & (\overline{A_a}Q + \overline{B_a}Y_0 + \overline{B_a}Y_1\omega_{max})^\intercal \\ \star & Q \end{bmatrix} > 0, \\
L \otimes Q + M \otimes (\underline{A_a}Q + \underline{B_a}Y_0 + \underline{B_a}Y_1\omega_{min}) + M^\intercal \otimes (\underline{A_a}Q + \underline{B_a}Y_0 + \underline{B_a}Y_1\omega_{min})^\intercal < 0, \\
L \otimes Q + M \otimes (\overline{A_a}Q + \overline{B_a}Y_0 + \overline{B_a}Y_1\omega_{max}) + M^\intercal \otimes (\overline{A_a}Q + \overline{B_a}Y_0 + \overline{B_a}Y_1\omega_{max})^\intercal < 0, \\
Q > 0.
\end{aligned} \tag{4.8}$$

Then, the system (4.2) *under the control law* (4.7)*, with*

$$\begin{aligned} L &= \begin{bmatrix} -r & c \\ c & -r \end{bmatrix}, \\ M &= \begin{bmatrix} 1 & 0 \\ 0 & 0 \end{bmatrix}, \\ K_0 &= Y_0 Q^{-1}, \\ K_1 &= Y_1 Q^{-1}. \end{aligned} \tag{4.9}$$

is asymptotically stable and the closed-loop poles are placed inside a disk with radius r and with center at coordinates c.

Proof. In order to demonstrate the proof, two conditions are necessary. The condition $V(x(k)) > 0$ holds from the assumption that $P > 0$. For the second condition $\Delta V(x(k)) < 0$, consider

$$\begin{aligned} \Delta V(x(k)) &= V(x(k+1)) - V((x(k)) < 0 \\ &= x(k+1)^\intercal P x(k+1) - x(k)^\intercal T P x(k) < 0 \end{aligned} \tag{4.10}$$

In closed loop, the augmented system (4.2) using the control law (4.7) takes the form of:

$$x(k+1) = (A_a + B_a(K_0 + K_1\omega))x(k). \tag{4.11}$$

Substituting in (4.10), we have

$$((A_a + B_a(K_0 + K_1\omega)x(k))^\intercal P((A_a + B_a(K_0 + K_1\omega)x(k)) - x(k)^\intercal P x(k) < 0,$$

which is equivalent to

$$(A_a + B_a(K_0 + K_1\omega)^\intercal P(A_a + B_a(K_0 + K_1\omega) - P < 0. \tag{4.12}$$

Making use of the Schur complement, defined in 2.1, we obtain:

$$\begin{aligned} \begin{bmatrix} P & (A_a + B_a K_0 + K_1\omega_i)^\intercal \\ \star & P^{-1} \end{bmatrix} > 0, \\ P > 0 \end{aligned} \tag{4.13}$$

Then, we may multiple both sides by a diagonal unit matrix $I \in \mathbb{R}^{n\times n}$, such that

$$\begin{bmatrix} Q & 0 \\ 0 & I_{n\times n} \end{bmatrix}, \tag{4.14}$$

where $Q = P^{-1}$, resulting in:

$$\begin{aligned} \begin{bmatrix} Q & QA_a^\intercal + Y_0^\intercal B_a^\intercal + Y_1^\intercal B_a^\intercal \omega_i \\ \star & Q \end{bmatrix} > 0, \\ , \\ Q > 0 \end{aligned} \tag{4.15}$$

where $Y_0 = K_0 Q$ and $Y_1 = K_1 Q$. Considering the polytopic approach, it is possible now to substitute ω_i by its vertices and their respective augmented matrices. By doing so, we now have

$$\begin{aligned}
\begin{bmatrix} Q & (\underline{A_a}Q + \underline{B_a}Y_0 + \underline{B_a}Y_1\omega_{min})^\intercal \\ \star & Q \end{bmatrix} > 0, \\
\begin{bmatrix} Q & (\overline{A_a}Q + \overline{B_a}Y_0 + \overline{B_a}Y_1\omega_{max})^\intercal \\ \star & Q \end{bmatrix} > 0, \\
Q > 0
\end{aligned} \tag{4.16}$$

Recalling the $\mathbb{D}$-stabilization structure defined in Equation (2.24), it may be adapted to the augmented system (4.2), its polytopic representation (4.5) and the control law (4.7). This results in the following equations:

$$\begin{aligned}
L \otimes Q + M \otimes (\underline{A_a}Q + \underline{B_a}Y_0 + \underline{B_a}Y_1\omega_{min}) + M^\intercal \otimes (\underline{A_a}Q + \underline{B_a}Y_0 + \underline{B_a}Y_1\omega_{min})^\intercal < 0, \\
L \otimes Q + M \otimes (\overline{A_a}Q + \overline{B_a}Y_0 + \overline{B_a}Y_1\omega_{max}) + M^\intercal \otimes (\overline{A_a}Q + \overline{B_a}Y_0 + \overline{B_a}Y_1\omega_{max})^\intercal < 0,
\end{aligned} \tag{4.17}$$

where, considering a disk region with radius r and center c in the complex plane,

$$L = \begin{bmatrix} -r & c \\ c & -r \end{bmatrix}, \qquad M = \begin{bmatrix} 1 & 0 \\ 0 & 0 \end{bmatrix}. \tag{4.18}$$

Finally, adding (4.17) to (4.16), we now have:

$$\begin{aligned}
\begin{bmatrix} Q & (\underline{A_a}Q + \underline{B_a}Y_0 + \underline{B_a}Y_1\omega_{min})^\intercal \\ \star & Q \end{bmatrix} > 0, \\
\begin{bmatrix} Q & (\overline{A_a}Q + \overline{B_a}Y_0 + \overline{B_a}Y_1\omega_{max})^\intercal \\ \star & Q \end{bmatrix} > 0, \\
L \otimes Q + M \otimes (\underline{A_a}Q + \underline{B_a}Y_0 + \underline{B_a}Y_1\omega_{min}) + M^\intercal \otimes (\underline{A_a}Q + \underline{B_a}Y_0 + \underline{B_a}Y_1\omega_{min})^\intercal < 0, \\
L \otimes Q + M \otimes (\overline{A_a}Q + \overline{B_a}Y_0 + \overline{B_a}Y_1\omega_{max}) + M^\intercal \otimes (\overline{A_a}Q + \overline{B_a}Y_0 + \overline{B_a}Y_1\omega_{max})^\intercal < 0, \\
Q > 0
\end{aligned} \tag{4.19}$$

It is possible to see that (4.19) is equal to (4.8). Hence, the proof is complete. □

Therefore, the resonant gain scheduling controller gains are obtained through the solution of the optimization problem 4.1 that uses the polytopic representation of the augmented system, which is defined by the system and the resonant system matrices, and a specific region in the complex plane. Moreover, the control law makes direct use of the frequency value in order to upgrade its action over the system.

4.3 Final Structure

The final structure diagram of the system control loop is depicted in Figure 10, where all the previous discussed strategies are represented as blocks, with $K_r(\omega) = K_{0r} + K_{1r}\omega$ and $K_x(\omega) = K_{0x} + K_{1x}\omega$. Note that this block diagram may be applied for both horizontal axes of the AFM, only requiring the appropriate changes regarding each axes particularities.

Figure 10 – Final structure of the proposed controller.

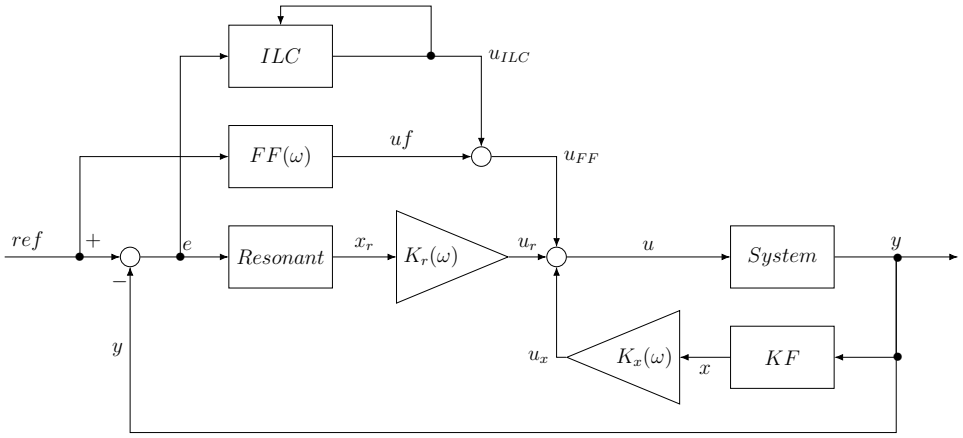

The diagram functioning can be describe as follows: first, the reference signal ref is compared to the system output measure y using a subtraction. This operation generates an error e, that becomes the input of the resonant system $Resonant$. The resonant system output is the resonant states, that are multiplied by their respective feedback gains $K_r(\omega)$, generating the control input u_r.

The feedforward block $FF(\omega)$ multiplies the reference by the inverse of the system gain, generating the control input u_{FF}. This gain is obtained, considering the following state-space model

$$\begin{aligned} x(k+1) &= Ax(k) + Bu(k) \\ y(k) &= Cx(k) \end{aligned} \tag{4.20}$$

where $x \in \mathbb{R}^n$ is the state vector, $u(k) \in \mathbb{R}$ is the control input, and A, B and C are definite and have appropriate dimensions, using the following equation (CHEN, 1999)

$$FF(\omega) = (-C(A - I + BK_x(\omega))^{-1}B)^{-1} \tag{4.21}$$

where $K_x(\omega) \in \mathbb{R}^n$ is the feedback gain computed through the optimization problem previously presented. By doing so, the feedforward block improves the tracking by compensating the system gain.

After the first iteration, the Iterative Learning Control block ILC starts to act, improving the feedforward response using the previous batches input and error information in order to generate the control input u_{ILC}. The block ILC represents the ILC

structure shown in Figure 6, recalling that it has memory blocks in order to store the past information about the error e and the control input u_{ILC}.

Despite the fact that the resonant gain scheduling controller is a discrete controller, the present work applies it in order to perform the reference tracking in a continuous system model. This procedure is done is order to simulate the control of a real system. In this context, the Kalman Filter is applied to estimated the system states x, necessary for the state-feedback structure, using the output measure y of the system block $System$. Therefore, the control input u_x is generated by the multiplication of the feedback gain $K_x(\omega)$ with the states estimated by the Kalman Filter block KF.

As the resonant states are produced using an "artificial" resonant system, their values are available during the entire simulation and need not be estimated. The block KF contains the Kalman Filter along with a discrete version of the AFM system, in order to generate the estimated states necessary for its functioning according to Algorithm 1.

The summation of all the four different control inputs is u, which is the continuous system input signal. One important remark is that the feedback gain varies according to the reference frequency, so the closed-loop system gain must be upgraded at each sample time in order that the feedforward controller operates correctly.

4.4 Final Considerations

This chapter presented the main contribution of the dissertation, the resonant gain scheduling controller for spiral reference tracking. The feedback controller was designed using a polytopic representation of the uncertain parameter and an augmented system composed by the controlled and the resonant systems matrices. The controller gains are obtained through an optimization problem structured using the Linear Matrix Inequalities approach. The chapter concluded with a block diagram of the system final structure, depicting and explaining the relation between the aforementioned resonant gain scheduling controller and the other strategies presented in the work, such as the Kalman Filter and the Iterative Learning Control.

5 Simulations Results

In this chapter, the results obtained through simulations are presented. First, the system used for the simulations is presented, being followed by its numerical representation. After, the reference signal used in the simulations is explained. In the sequence, a comparative controller composed of a proportional-integral controller is detailed and its parameters defined, being followed by the proposed controller parametrization.

Finally, the graphical results obtained are presented for the proportional-integral controller, the resonant gain scheduling controller and its respective applications with the Iterative Learning Control. The analysis on error reduction, ILC stability and errors and control inputs signals are also presented. In the sequence, the section is concluded with the numerical results of the simulation, which allow a further discussion in the controllers performances.

5.1 Simulation parameters

The section presents the main information about the numerical simulations performed in order to demonstrate the proposed resonant gain scheduling controller and the Iterative Learning Control performance. First, it details the numerical model of a AFM nanopositioner system used in the simulations. After, a new scanning reference pattern is presented, based in the OPT pattern definitions.

Then a comparative proposed controller, composed of a proportional-integral controller plus a feedforward and Iterative Learning Control structure, is presented, in order to allow a performance comparison. The software used to perform the simulation was the Matlab version 2011b. The LMIs programming was performed using the Yalmip toolbox (LOFBERG, 2004), and they were solved using the semidefinite programming package SDPT3 (TOH; TODD; TUTUNCU, 1999).

5.1.1 Microelectromechanical Systems

The Atomic Force Microscopes operation depends directly of its nanopositioning system. This equipment is responsible for generating the microscope x-y-z scanning movements necessary for the sample imaging. The most common nanopositioner used in AFM applications is the piezoelectric tube, due its simple structure and low cost (YABLON, 2014). Basically, they consist in cylinders with four internal and external metal electrodes, the latter divided into four quadrants. In order to generate movement, a voltage must be

applied to one of the external electrodes, resulting in the bending of the tube, which is translated into motion (TSUKRUK; SINGAMANENI, 2011).

Nevertheless, traditional piezoelectric tubes may present limitations like cross-coupling between the axes and limited bandwidth (MAROUFI; MOHEIMANI, 2016). In this context, the microelectromechanical systems (MEMS) nanopositioners received more attention in recent researches. The MEMS is piezoelectric tube with advantages such that high bandwidth, reduce footprints (smaller dimensions) and low fabricating costs for bulk production (BAZAEI et al., 2016).

The numerical system used in the simulations is a model obtained from a two degree of freedom (DOF) MEMS nanopositioner described in (MAROUFI; MOHEIMANI, 2016). In order to augment the system damping, the authors applied a damping controller in the form of

$$C(s) = \frac{5s}{s + 88000}, \tag{5.1}$$

using an analogue circuit and applied in the MEMS system through a feedback loop.

The state-space continuous matrices that describe the linear time-invariant SISO model of the damped nanopositioner, used for both axes simulations, are given by (BAZAEI; MAROUFI; MOHEIMANI, 2017), with $D_c = 0$:

$$A_c = \begin{bmatrix} -5649 & 20677 & -644 & -2813 & -5007 \\ -20677 & -20979 & 1503 & 12935 & 21177 \\ 644 & 1503 & -170 & -319611 & -14364 \\ -2813 & -12935 & 319611 & -4668 & -9134 \\ -5007 & -21177 & 14364 & -9134 & -18127 \end{bmatrix}, \; B_c = \begin{bmatrix} 90 \\ 104 \\ -5 \\ 24 \\ 42 \end{bmatrix}, \; C_c = \begin{bmatrix} 89 \\ -104 \\ 5 \\ 24 \\ 42 \end{bmatrix}^{\intercal}. \tag{5.2}$$

The discrete version of the system and all other discretizations along the work of were obtained through the Tustin discretization method, using a sample time of $T_s = 20\mu$s[1]. The sample time value was chosen according to (ZIEGLER et al., 2017).

5.1.2 Repetitive Archimedean Spiral

In order to perform the simulations and analyze the controller performance, the present work proposes the tracking of the so-called Repetitive Archimedean Spiral (RAS). In this pattern, the previously presented OPT pattern is modified such as the generated reference is composed of a closed path: when each of the spiral axes signals ends, they are mirrored in such a way that the spiral returns to its center.

These spirals may be applied, for example, in the monitoring of living samples through AFM, where a continuous image acquisition is necessary. In this context, the

[1] During the simulations, the Tustin method demonstrated the best results for the LMIs procedures, being chosen as the work method.

Iterative Learning Control justifies its application, as the same reference pattern is continuously repeated over the iterations.

The RAS pattern uses the same procedures and parameters presented in the Background chapter for the OPT pattern. After generating spiral x and y components, their signal are appropriately mirrored such that when combined, they generate a spiral with a closed path. Figure 11 presents the RAS pattern used in the simulations of the next sections. The RAS parameters are: radius $R_s = 1\mu$m, spiral total time $T = 0.0074s$, switching time $t_{*0} = 7.8 \times 10^{-4}s$, constant linear velocity $v = 0.00445m/s$ and constant angular velocity of $\omega = 6000\pi$.

Figure 11 – RAS pattern with $R_s = 1\mu$m, $M = 5$ and $P = 1 \times 10^{-7}$, and its respective x and y axes components. The black lines represent first half of the pattern, while the gray ones represent the last half.

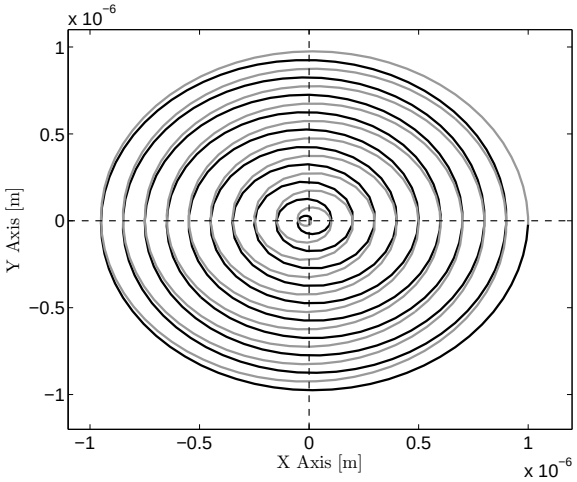

(a) RAS pattern with $R_s = 1\mu$m, $M = 5$ and $P = 1 \times 10^{-7}$.

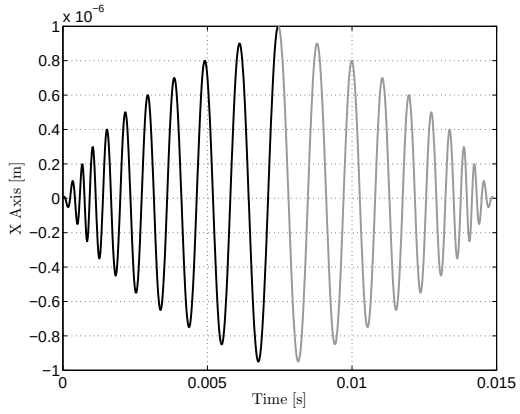

(b) RAS pattern x axis.

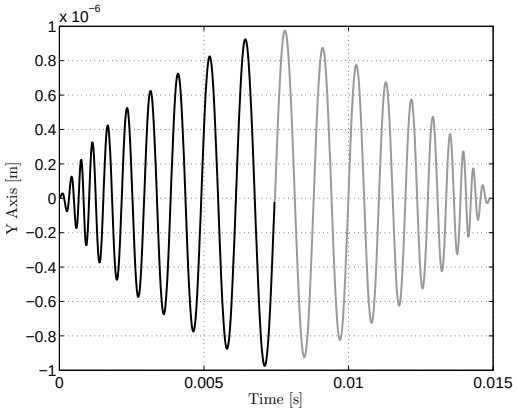

(c) RAS pattern y axis.

Figure 12 presents the linear and angular velocities signals for the previous RAS reference. It is possible to see that the angular velocity starts in a constant value switching to a varying function after the switching time. On the other hand, the linear velocity varies in the beginning of the spiral until the switching time, where it maintains a constant value.

After half of the reference time, both velocity signals are mirrored, as defined by the RAS pattern.

Figure 12 – RAS pattern angular and linear velocities signals.

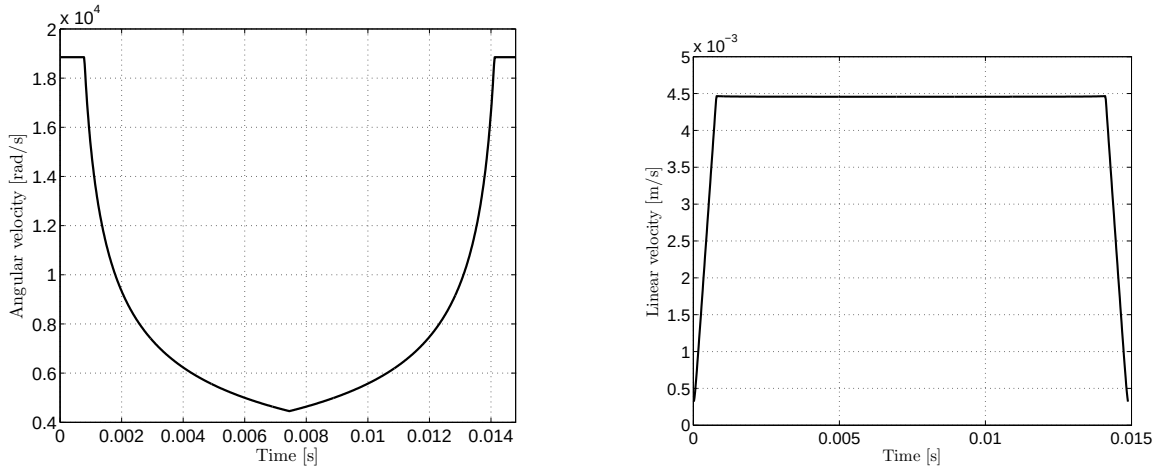

(a) Angular velocity. (b) Linear velocity.

5.1.3 Proportional-Integral Controller plus Iterative Learning Control

In order to perform a performance comparison, a proportional-integral (PI) controller with feedforward will be also simulated along with the resonant gain scheduling controller. Aiming to improve the text reading, from now on this controller will be refereed only as proportional-integral controller. As the numerical system (5.2) is considered the same for both axes, the control parameters further defined are also applied for both axes.

Commonly, atomic force microscopes operate in open-loop or with proportional-integral controllers (BARÓ; REIFENBERGER, 2012; MEYER; HUG; BENNEWITZ, 2004). According to Habibullah, Pota e Petersen (2014a), the correct scanning of spiral patterns is not possible in open-loop, as the amplitude dependent phase shifts may lead to inaccurate tracking. Nevertheless, the PI controllers are a good cost/benefit option for most applications (ŻAK, 2003), such as the AFM scanners (WU; ZOU; SU, 2009).

The continuous PI parallel structure is defined as (ŻAK, 2003):

$$u(t) = K_p e(t) + K_i \int_0^t e(\tau) d\tau, \tag{5.3}$$

where K_p is the proportional gain, K_i is the integral gain, and the error $e(t) = r(t) - y(t)$ is obtained by the subtraction of the reference signal $r(t)$ and the output signal $y(t)$.

As the present work deals with discrete controllers, the PI must be represented as a discrete function. Considering that $u(0) = 0$, a possible representation is given as follows:

$$u(k) = K_p e(k) + K_i T_s \sum_{i=1}^{N} e_i(k). \tag{5.4}$$

In discrete time, the integral term becomes a summation, that accumulates the error values over the N samples, spaced by the sample time T_s. The PI parameters were tuned maintaining a balance between bandwidth and phase margin, which resulted in $K_p = 1$ and $K_i = 10000$. The feedforward gain compensation is obtained using the procedure of the resonant gain scheduling controller, with the exception that the system does not have any state feedback gain.

The Iterative Learning Control was designed using the previously presented procedure in section 3.2, where the learning function is designed such that $L(z) = (S(z)G(z))^{-1}$, while the Q-filter $Q(z)$ must assure the stability. First, the system transfer function was obtained directly from the discrete representation of the system presented in (5.2), through the relation $G_1(z) = C(zI_{n\times n} - A)^{-1}B + D$.

$$G_1(z) = \frac{0.01984z^5 + 0.0861z^4 + 0.1271z^3 + 0.06698z^2 - 0.006496z - 0.01264}{z^5 - 0.4051z^4 - 0.7987z^3 + 0.08418z^2 + 0.8281z - 0.427}. \tag{5.5}$$

For the PI controller, the transfer function was defined as the following transfer function:

$$C_1(z) = \frac{1.1z - 0.9}{z - 1}. \tag{5.6}$$

The learning function $L_1(z) = (G_1(z)S_1(z))^{-1}$, where $S_1(z) = (1 + C_1(z)G_1(z))^{-1}$, was first defined as:

$$L_1(z) = \frac{a(z)}{b(z)}, \tag{5.7}$$

where

$$\begin{aligned} a(z) =&(z - 0.7215)(z - 0.8821)(z^2 - 1.319z + 0.5981)(z^2 - 1.413z + 0.7697) \\ &(z - 0.6391)(z^2 + 1.636z + 0.9896)(z^2 + 1.634z + 0.9888) \end{aligned} \tag{5.8}$$

and

$$\begin{aligned} b(z) =&(z + 1.0002)(z - 1.0006)(z - 0.7215)(z - 0.3487)(z^2 - 1.319z + 0.5981) \\ &(z + 1.911)(z^2 + 1.777z + 0.9563)(z^2 + 1.636z + 0.9896) \end{aligned} \tag{5.9}$$

An analysis of the transfer function revealed that the denominator has unstable poles at 1.0006, -1.911 and -1.0002. These unstable poles are removed from the filter $L(z)$, and, in order to maintain the transfer function causality, two fast poles are inserted in -0.05 and -0.04. Finally, the learning function becomes:

$$L_1(z) = \frac{a(z)}{b(z)}, \tag{5.10}$$

where

$$\begin{aligned} a(z) =&(z - 0.7215)(z - 0.8821)(z^2 - 1.319z + 0.5981)(z^2 - 1.413z + 0.7697) \\ &(z - 0.6391)(z^2 + 1.636z + 0.9896)(z^2 + 1.634z + 0.9888) \end{aligned} \tag{5.11}$$

and

$$\begin{aligned} b(z) =&(z-0.7215)(z-0.3487)(z+0.05)(z+0.04)(z^2-1.319z+0.5981) \\ &(z-0.3487)(z^2+1.777z+0.9563)(z^2+1.636z+0.9896) \end{aligned} \tag{5.12}$$

In order to respect the ILC stability condition, a low-pass filter was designed with cut-off frequency of 6×10^4 rad/s. Its discrete transfer function is given by

$$Q_1(z) = \frac{0.375z + 0.375}{z - 0.25}. \tag{5.13}$$

Recalling the ILC properties from Theorem 3.3, stability is guaranteed if $|Q_2(z)(1-G_2(z)S_2(z)L_2(z))| < 1$. This condition can be better visualized using a Bode diagram, where it is equivalent to the magnitude does not pass the 0 dB level (BOEREN et al., 2016). Figure 13 shows the Bode magnitude response for three different functions: the condition $|1-G_1(z)S_1(z)L_1(z)|$, the Q-Filter and their combination $|Q_1(1-G_1(z)S_1(z)L_1(z))|$. It is possible to see that the condition from Theorem 3.3 is respected, as the magnitude signal is always lower than 0 dB, i.e., lower than one.

Figure 13 – PI plus ILC controller bode magnitude responses of: the designed Q-Filter $Q_1(z)$, $(1 - G_1(z)S_1(z)L_1(z))$ and $(Q_1(1 - G_1(z)S_1(z)L_1(z)))$.

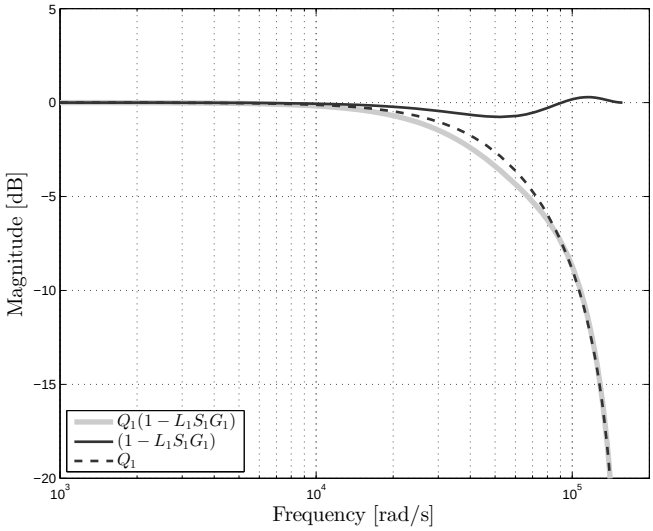

5.1.4 Resonant Gain Scheduling plus Iterative Learning Control parameters

The Kalman Filter matrices that represent the system and sensors uncertainties and the states initial estimation covariance, are given, respectively, by $\mathcal{R} = I_{5\times5}$, $\mathcal{Q} = 1$ and $\Sigma = I_{5\times5}$. The feedback gains for the resonant gain scheduling controller were computed using the procedure detailed in Chapter 4. According to the RAS reference parameters previously defined, the frequency set is defined by equation (5.14).

$$\omega \in \left[\underline{\omega} = 4457.2\tfrac{rad}{s},\ \ \overline{\omega} = 6000\pi\tfrac{rad}{s}\right], \tag{5.14}$$

The main parameters were the discretized version of the system (5.2), the RAS reference frequency set (5.14) and the $\mathbb{D}$-stabilization disk region with radius 0.96 and the center in the complex plane origin. The gains are given by equation (5.15). Recalling that the numerical system, defined in (5.2) is used for both axes, the same control parameters will also be applied in both axes.

$$\begin{aligned} K_0 &= \begin{bmatrix} -0.02012 & 0.00422 & -0.00158 & -0.00425 & 0.00056 & 3.58858 & 3.79579 \end{bmatrix} \\ K_1 &= 10^{-4} \times \begin{bmatrix} -0.00208 & 0.00075 & 0.00072 & 0.00044 & -0.00015 & -0.14602 & 1.07701 \end{bmatrix} \end{aligned} \tag{5.15}$$

In order to present the ILC parameters, first it is necessary to present the system closed-loop and the controller transfer functions. They are defined for the highest frequency case, i.e. $\omega = \overline{\omega}$. Using the system presented in (5.2) and the feedback gains presented in (5.15), the closed-loop discrete transfer function $G_2(z) = C(zI_{n\times n} - A + B(K_{0x} + K_{1x}\overline{\omega}))^{-1}B + D$ was defined as

$$G_2(z) = \frac{0.01984z^5 + 0.08658z^4 + 0.127z^3 + 0.06699z^2 - 0.006428z - 0.01265}{z^5 - 0.381z^4 - 0.8043z^3 + 0.0844z^2 + 0.8315z - 0.4276}. \tag{5.16}$$

As presented in the Resonant Gain Scheduling chapter, the controller gains also affects the resonant system. Therefore, using the schematic of Chapter 4, it is possible to see that the controller $C(z)$, for $\overline{\omega}$, is given by

$$C_2(z) = C_r(A_r + B_r(K_{0r} + K_{1r}\overline{\omega}))^{-1}B_r = \frac{10^{-5} \times (0.182z^2 - 0.7698z + 1.096)}{z^2 - 8.092z + 6.023}. \tag{5.17}$$

The learning function of the ILC controller was designed as $L_2(z) = (G_2(z)S_2(z))^{-1}$, recalling that $S_2(z) = (1 + G_2(z)C_2(z))^{-1}$. Using the previous transfer functions, the following learning function was designed:

$$L_2(z) = \frac{c(z)}{d(z)}, \tag{5.18}$$

where

$$\begin{aligned} c(z) =& (z - 0.8293)(z - 0.7077)^2(z^2 - 1.321z + 0.6053)^2 \\ & (z - 7.263)(z^2 + 1.648z + 0.9981)^2 \end{aligned} \tag{5.19}$$

and

$$\begin{aligned} d(z) =& (z - 7.263)(z + 2.035)(z + 0.9156)(z - 0.8293)(z - 0.7077)(z - 0.3485) \\ & (z^2 - 1.321z + 0.6053)(z^2 + 1.761z + 0.982)(z^2 + 1.648z + 0.9981) \end{aligned} \tag{5.20}$$

An analysis of the transfer function denominator reveals that there are unstable poles at 7.263 and -2.035 and an unstable zero at 7.263. In order to keep the filter stable

and causal, the unstable poles and zero are removed from the filter and a fast pole is inserted in -0.05. With these modifications, the learning function now becomes:

$$L_2(z) = \frac{c(z)}{d(z)}, \tag{5.21}$$

where

$$c(z) = (z - 0.9991)^4(z - 0.8293)(z - 0.778)^4(z - 0.7077)^2 \tag{5.22}$$

and

$$\begin{aligned} d(z) =&(z - 0.9156)(z - 0.9909)^2(z - 0.9991)^2(z - 0.8293) \\ &(z - 0.7077)(z - 0.3485)(z + 0.05)(z - 0.778)^2 \end{aligned} \tag{5.23}$$

A low-pass filter, with cut-off frequency of 4×10^4 rad/s, was designed in order to respect the stability condition for the ILC. The filter transfer function is defined as

$$Q_2(z) = \frac{0.2857z + 0.2857}{z - 0.4286}. \tag{5.24}$$

Similarly as presented for the PI controller, Figure 14 shows the Bode magnitude response for three different functions: the condition $|1 - G_2(z)S_2(z)L_2(z)|$, the Q-Filter and their combination $|Q_2(1 - G_2(z)S_2(z)L_2(z))|$. According to Theorem 3.3, stability is guaranteed, as the condition $|Q_2(z)(1 - G_2(z)S_2(z)L_2(z))| < 1$ is satisfied using the designed Q-filter.

Figure 14 – Resonant Gain Scheduling plus ILC controller bode magnitude responses of: the designed Q-Filter $Q_2(z)$, $(1 - G_2(z)S_2(z)L_2(z))$ and $(Q_2(1 - G_2(z)S_2(z)L_2(z)))$.

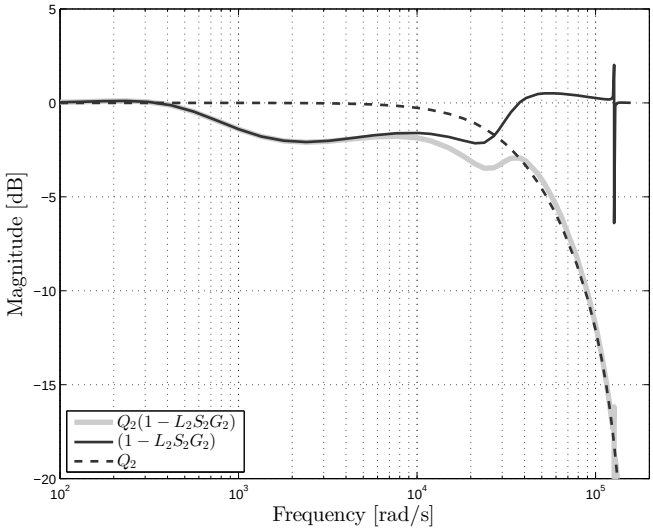

5.2 Proportional-Integral Controller Results

This section presents the graphical results obtained by the simulation of the presented numerical model and the RAS reference using the proportional-integral controller. Figure 15 presents the output and input responses, of both axes, for the proportional-integral controller. The controller was not able to achieve a satisfactory tracking of the sinusoidal reference, which generated a visible magnitude error in the output signal.

Figure 15 – RAS x and y axes output and input responses for the proportional-integral controller. The vertical lines represent the switching times.

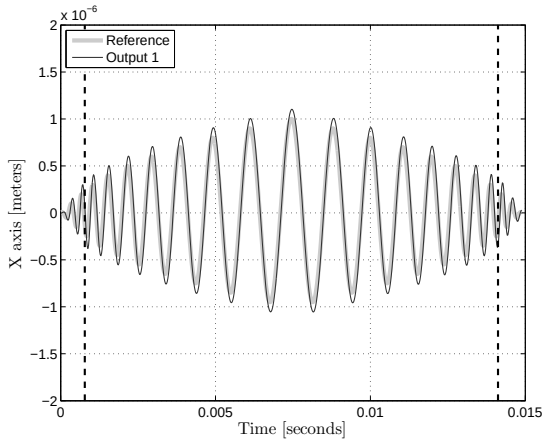

(a) X axis reference and output responses.

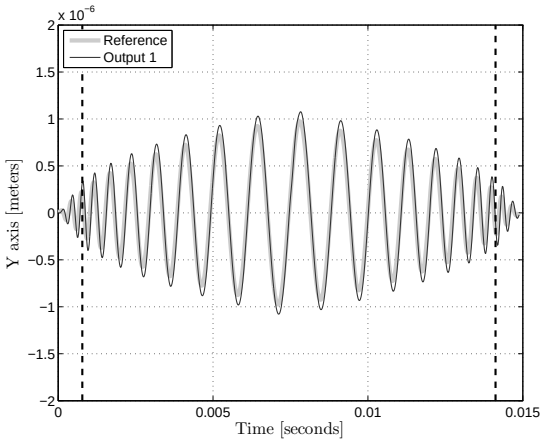

(b) Y axis reference and output responses.

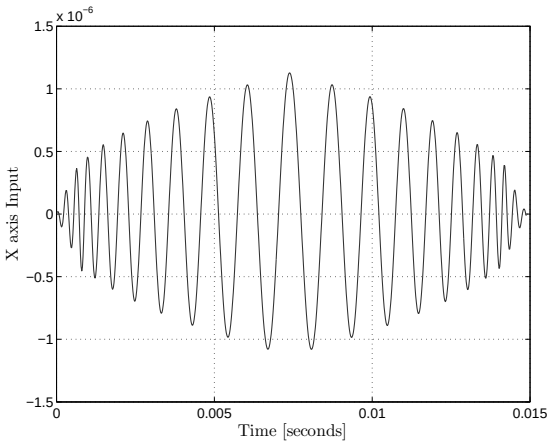

(c) X axis input response.

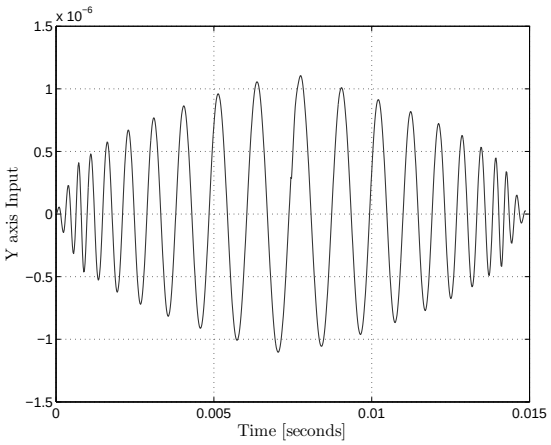

(d) Y axis input response.

The error signals from each one of the spiral components are depicted in Figure 16, along side with the respective generated spiral. In order to make the plots cleaner, from now on only half of the RAS pattern is depicted. As expected from its components, the spiral presents a poor tracking in the center (beginning) of the signal. Although the reference tracking looks correct after half of the graphic radius, actually the output has a loop phase lag, generated in the center. This fact created the difference between the reference and the output in the periphery (half) of the spiral.

Figure 16 – RAS error signals for both axes and spiral response for the proportional-integral controller.

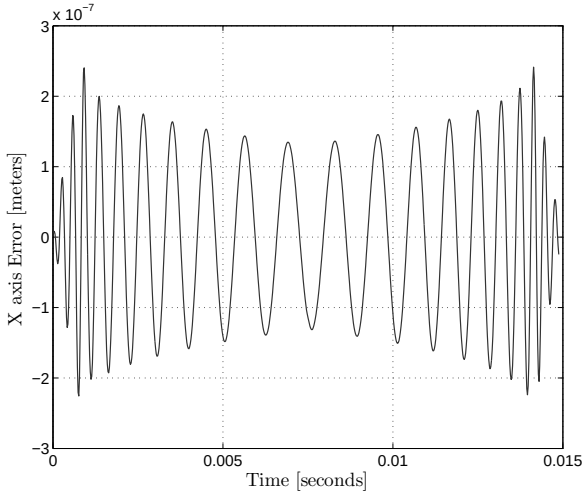

(a) X axis error signal.

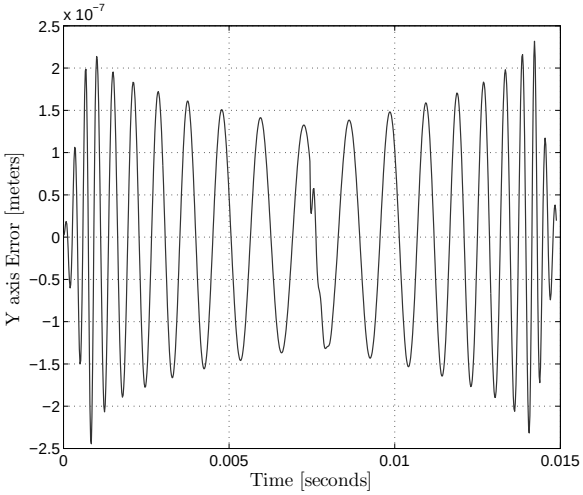

(b) Y axis error signal.

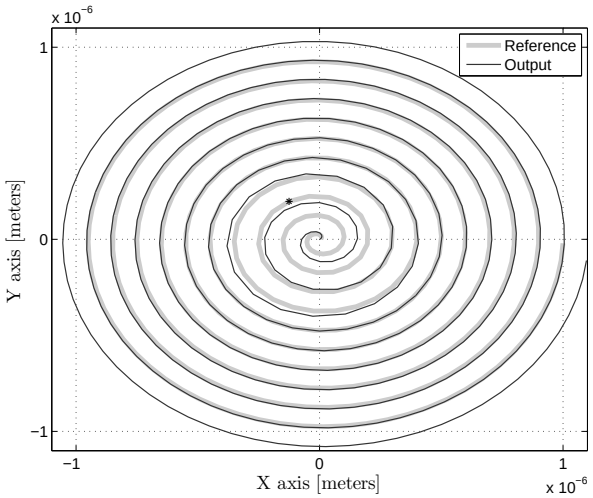

(c) RAS spiral reference an output responses, between $\pm 1.1\mu$, for the proportional-integral controller. The black point represents the frequency switching time.

5.3 Proportional-Integral Controller plus Iterative Learning Control Results

Now, the results regarding the addition of the Iterative Learning Control to the proportional-integral controller are presented. In Figure 17 the output responses for both RAS pattern axes, along side with its respective control inputs are depicted. The presented graphics correspond to the last iteration outputs and control inputs computed after 120 iterations. It is possible to see that the ILC improved the signals tracking, reducing the previous magnitude error.

The ILC effect on the tracking can be better visualized in Figure 18, where the

Figure 17 – RAS x and y axes output and input responses for the proportional-integral plus Iterative Learning Control controller (last iteration). The vertical lines represent the switching times.

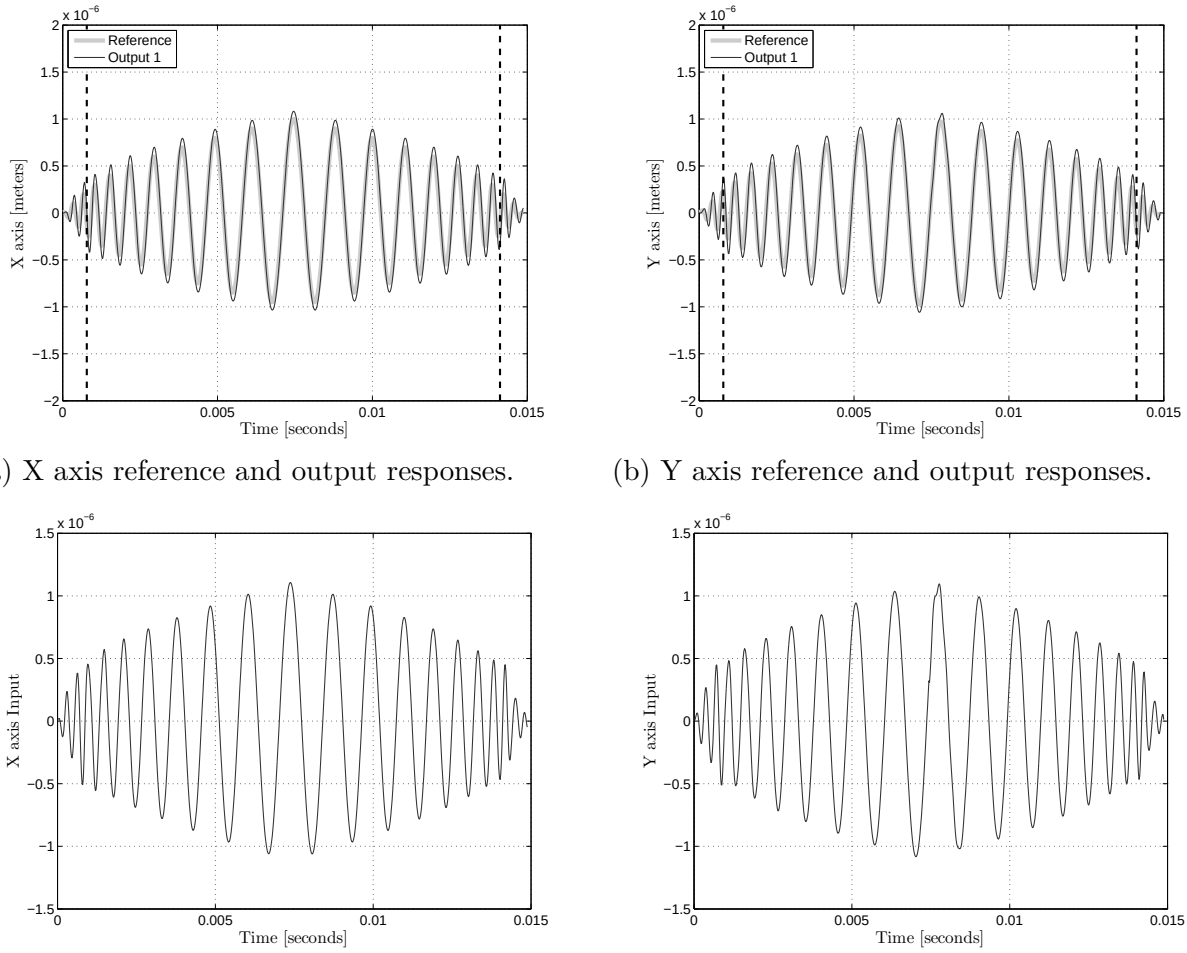

(a) X axis reference and output responses.

(b) Y axis reference and output responses.

(c) X axis input response.

(d) Y axis input response.

error signals for both axes are presented for the first and last iteration. The spiral response generated by the last iteration is also depicted. As expected, the ILC was able to reduce the tracking error, improving the control performance in general. While the spiral response still has a phase lag, it is smaller than without the ILC addition.

Another important result is the ILC error behavior along the performed iterations. As the reference is repeatedly applied, it is expected that the error decreases over the batch with stable dynamics, as proposed in the ILC design. The *rms* tracking error in each iteration, i.e. E_{rms}, is computed using the following equation

$$E_{rms} = \sqrt{\frac{\sum_{i=1}^{N}(\mathbf{r}_i - \mathbf{y}_i)^2}{N}}, \tag{5.25}$$

where $\mathbf{r}$ is the reference signal vector, $\mathbf{y}$ is the output vector, and $N = T/T_s$ is the number of samples.

Figure 18 – RAS error signals for both axes and spiral response for the proportional-integral controller plus Iterative Learning Control.

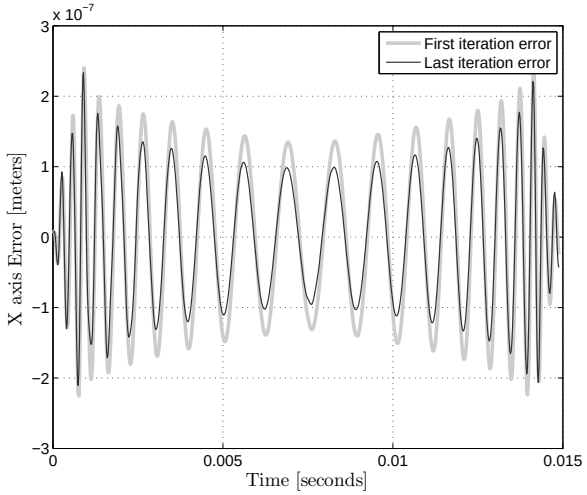

(a) X axis error signal for the first and last iteration.

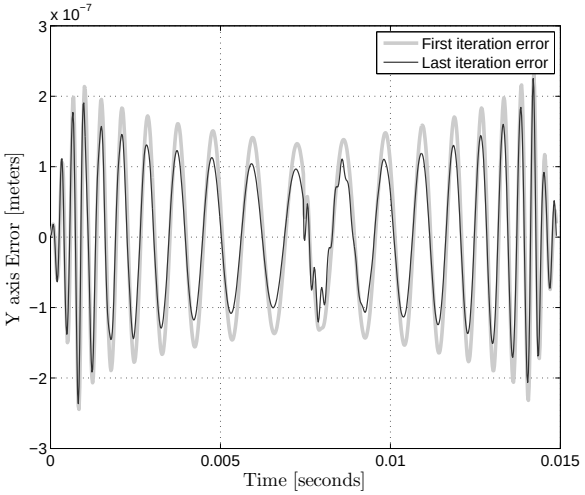

(b) Y axis error signal for the first and last iteration.

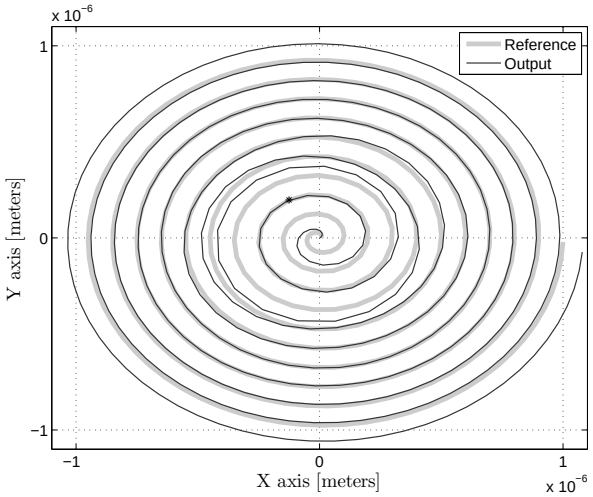

(c) RAS spiral reference and output responses, between $\pm 1.1\mu$, for the comparative controller plus Iterative Learning Control (last iteration). The black point represents the frequency switching time.

In Figure 19 the *rms* error evolution over the iterations is presented for both axes. Just as expected from the ILC design, the error presents a stable dynamics, achieving a constant value after 100 iterations.

Figure 19 – RAS x and y axes *rms* errors over the iterations for the proportional-integral controller plus Iterative Learning Control.

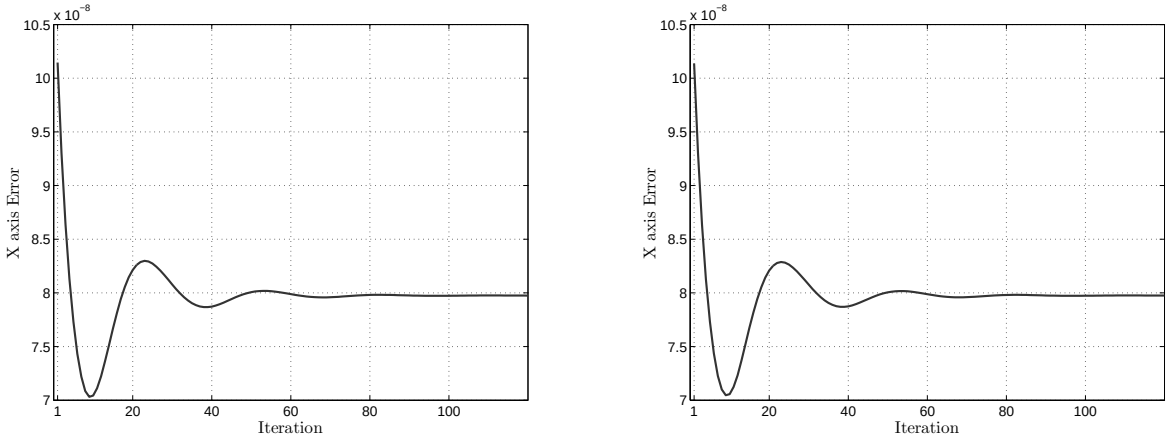

(a) X axis *rms* error over the iterations.

(b) Y axis *rms* error over the iterations.

5.4 Resonant Gain Scheduling Controller Results

Now, the graphical results regarding the main contribution of this work, i.e. the resonant gain scheduling controller, are presented. In Figure 20, the output and input responses for both x and y axes are depicted. As it is possible to see, the proposed controller was able to achieve satisfactory results for the RAS pattern tracking. Analysing the control input signals, it is notable that the resonant controller does not require larger control efforts than the proportional-integral controller.

Figure 21 presents the error signals for both axes and the spiral response. It is possible to see that the errors are smaller than the ones obtained with the proportional-integral controller. The spiral center is a critical part of the tracking, as the higher angular velocity values are located there. The proportional-integral controller is not able to deal with this high speed transitions. On the other hand, the resonant controller is capable of following the sinusoidal signal, as it takes the signal frequency in consideration.

Figure 20 – RAS x and y axes output and input responses for the resonant gain scheduling controller. The vertical lines represent the switching times.

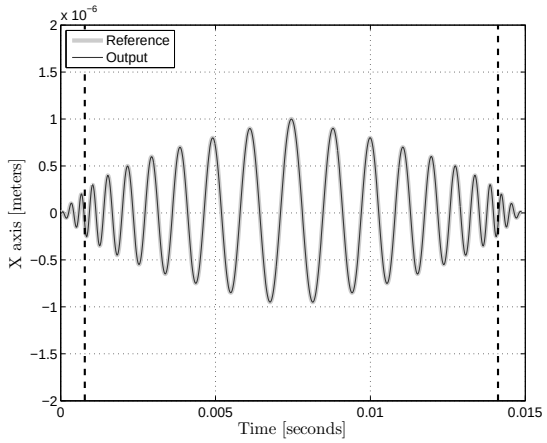

(a) X axis reference and output responses.

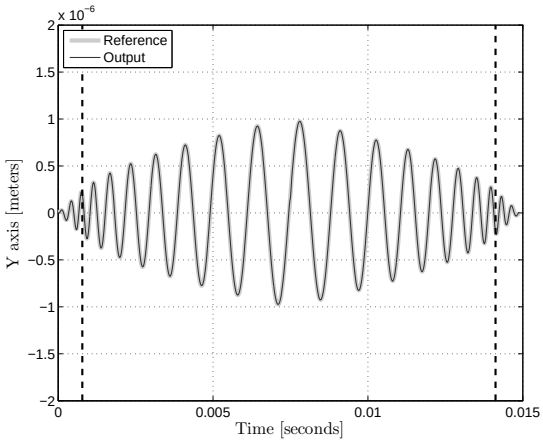

(b) Y axis reference and output responses.

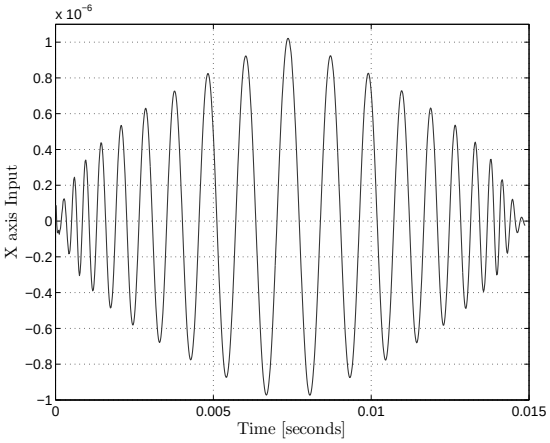

(c) X axis input response.

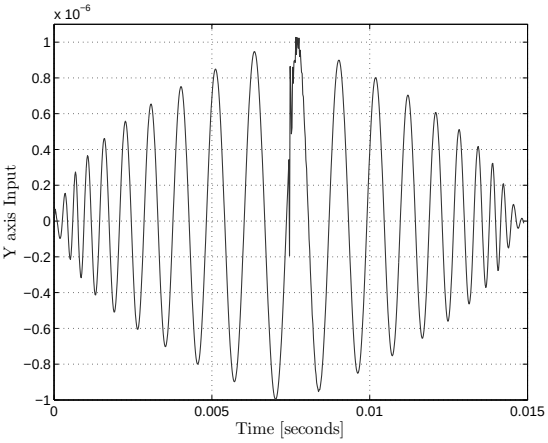

(d) Y axis input response.

Figure 21 – RAS error signals for both axes and spiral response for the resonant gain scheduling controller.

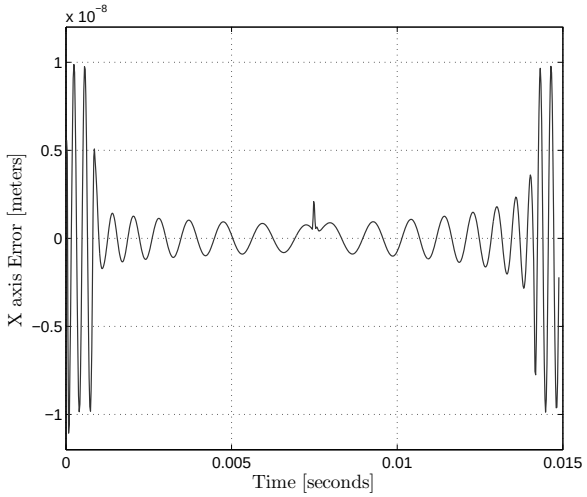

(a) X axis error signal.

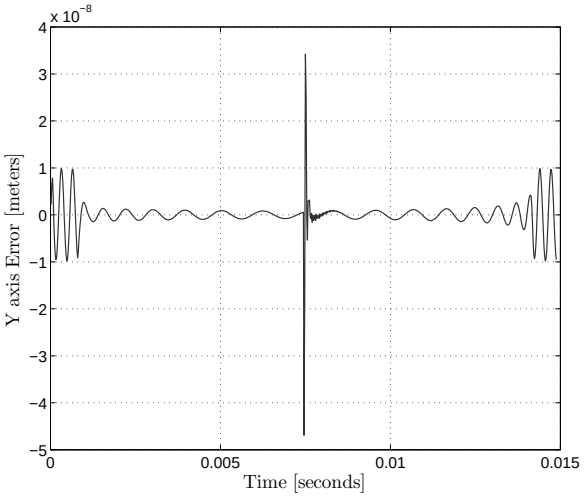

(b) Y axis error signal.

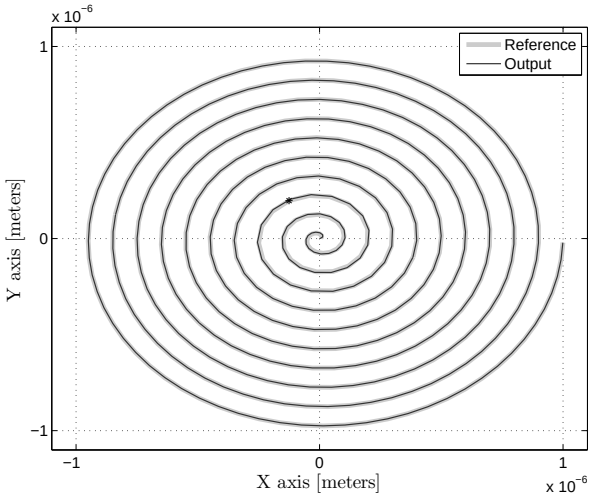

(c) RAS spiral reference and output responses, between $\pm 1.1\mu$, for the resonant gain scheduling controller. The black point represents the frequency switching time.

5.5 Error reduction through the attenuation of non-smooth areas

When the RAS signal is generated, a small non-smooth area is created in the point where the spiral is mirrored. As the proposed controller makes use of the sinusoidal dynamics of the reference, any rough area may degrade the controller performance. This behavior can be observed in Figure 21, where the x and y axes errors graphics depict two areas with peaks in the signal due to this non-smooth area.

A possible solution is to filter the reference signal in order to eliminate any irregular sections of the signal. Although this procedure may reduce the problem, the filter must be projected such that the reference does not lose its interesting properties.

In order to exemplify the idea, two different low-pass filters will be applied to the previously used reference. The first one, F_{B1}, has a cut-off frequency of 1×10^5 rad/s and the second one, F_{B2}, 1×10^4 rad/s. The respective transfer functions are given by

$$\begin{aligned} F_{B1}(z) &= \frac{0.5z + 0.5}{z} \\ F_{B2}(z) &= \frac{0.09091z + 0.09091}{z - 0.8182} \end{aligned} \tag{5.26}$$

Figure 22 presents a comparison between of the Y axis error graphics generated by the reference filtered by F_{B1} and F_{B2}. As it is possible to see, the filters helped to achieve smaller errors than the original one, depicted in Figure 21b. The more aggressive the filter, i.e. the more frequencies attenuated, the more reduced was the peak at half of the signal.

Nevertheless, if the filter is too aggressive, it may affect frequency components that are necessary in order to form the sinusoid signal, such that the spiral radius and loops are not respected any more. Figure 23 presents the attenuated spirals, generated after the filtering generated by the functions F_{B1} and F_{B2}, compared to the original RAS pattern. As expected, the attenuation of the filter F_{B2} degraded the spiral dynamics more than the filter F_{B1}.

Figure 22 – Y axis error comparison for different filtered references.

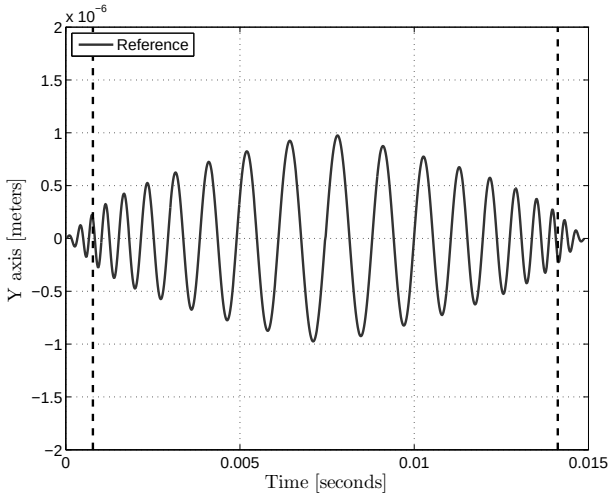

(a) References for the y axis filtered by F_{B1}.

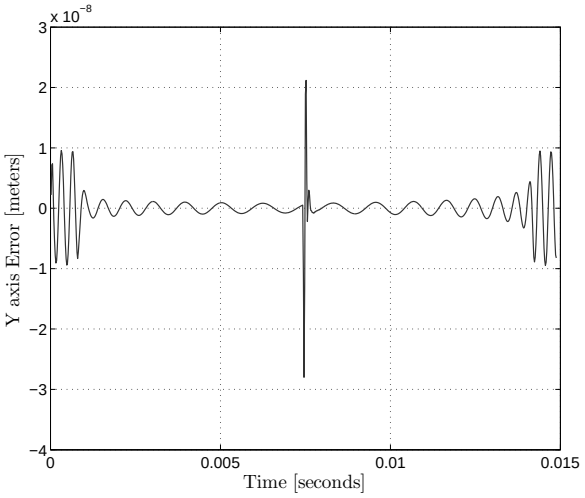

(b) Error for the y axis reference filtered by F_{B1}.

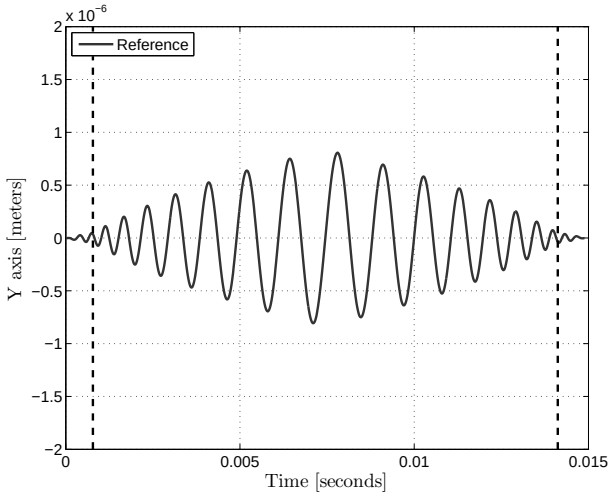

(c) Reference for the y axis filtered by F_{B2}.

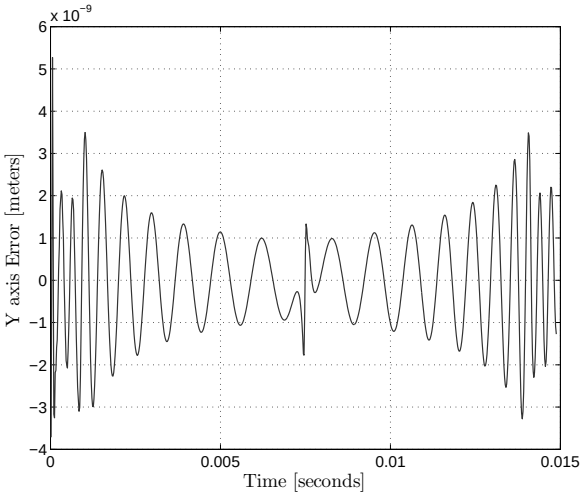

(d) Error for the y axis reference filtered by F_{B2}.

Figure 23 – Effect of the filtering over the spirals for tracking error attenuation.

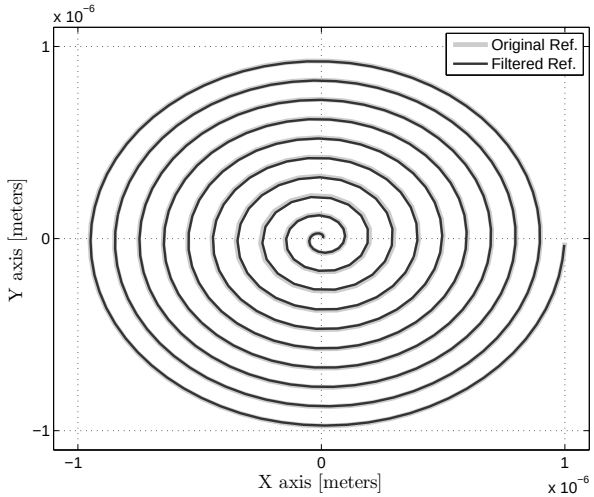

(a) Spiral generated after its components being filtered by F_{B1}.

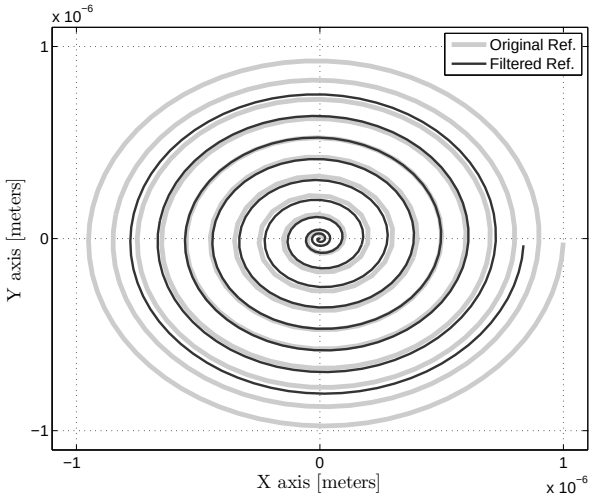

(b) Spiral generated after its components being filtered by F_{B2}.

5.6 Resonant Gain Scheduling Controller plus Iterative Learning Control Results

This section presents the graphical results for the proposed resonant gain scheduling controller with the Iterative Learning Control addition. Figure 24 depicts the output and input responses, of both axes, for the proposed controller with ILC after 300 iterations. As the error already was small, the ILC was not able to improve significantly the tracking results.

Figure 24 – RAS x and y axes output and input responses for the resonant gain scheduling controller plus the Iterative Learning Control (last iteration). The vertical lines represent the switching times.

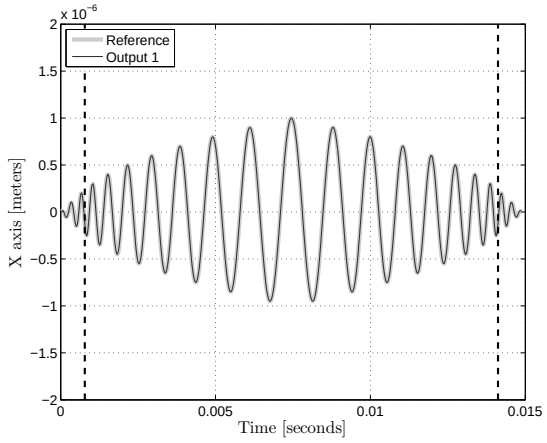

(a) X axis reference and output responses.

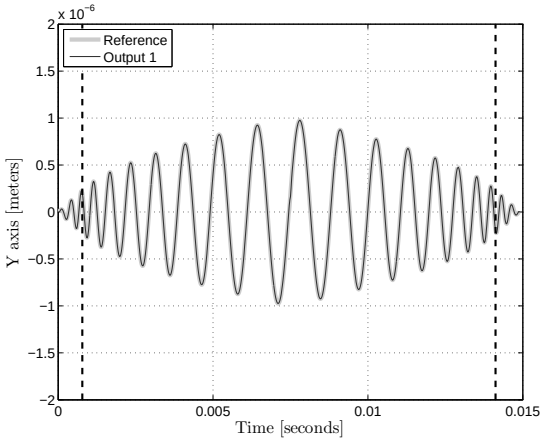

(b) Y axis reference and output responses.

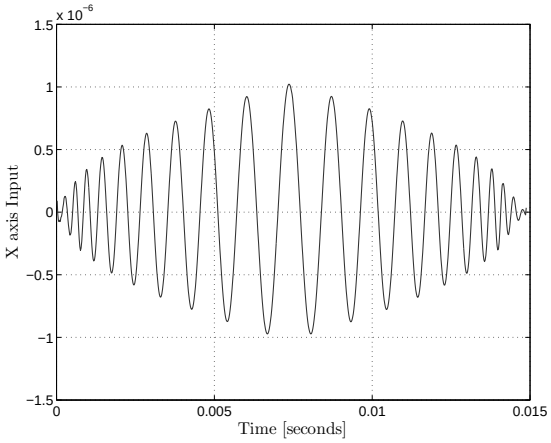

(c) X axis input response.

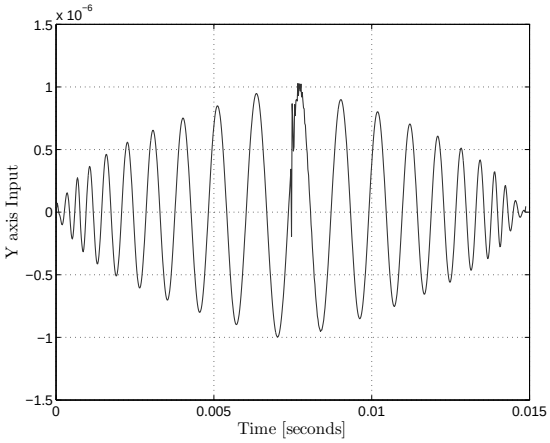

(d) Y axis input response.

Figure 25 presents the error signals, of both x and y axes, for the first and last iterations, along side with the spiral response for the last iteration. It is possible to see a small performance improvement with the ILC addition. As the resonant gain scheduling already had good performance, the ILC was not able to achieve greater improvement.

In Figure 26 the *rms* error evolution over the iterations is depicted. These results

Figure 25 – RAS error signals for both axes and spiral response for the resonant gain scheduling controller plus the Iterative Learning Control.

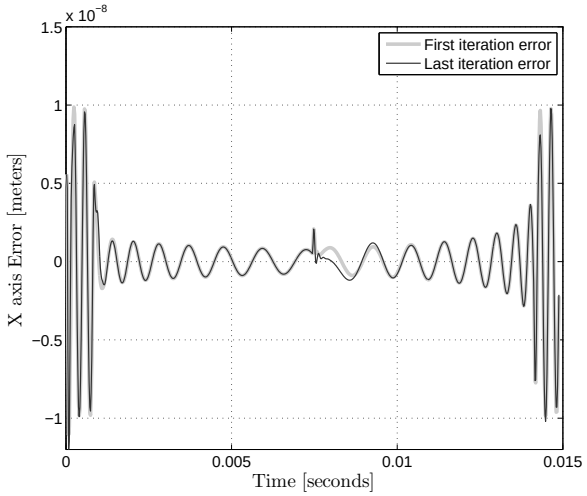

(a) X axis error signal for the first and last iteration.

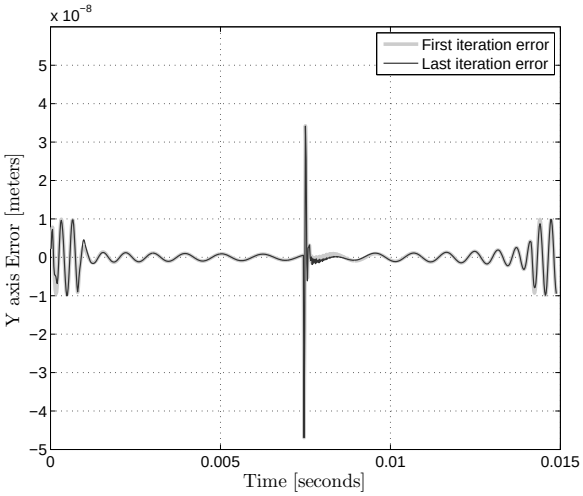

(b) Y axis error signal for the first and last iteration.

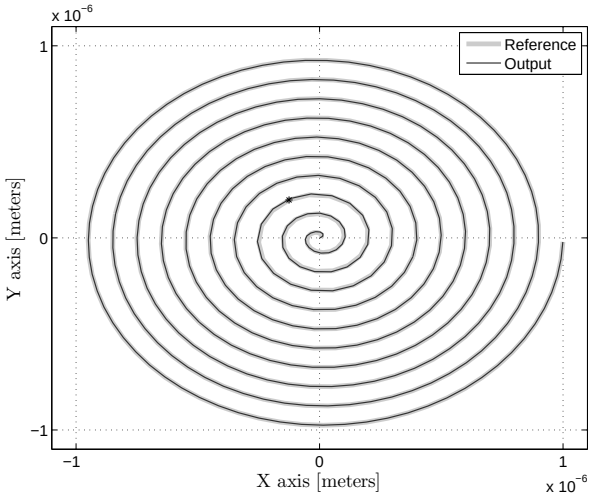

(c) RAS spiral reference and output responses, between $\pm 1.1\mu$, for the proposed controller plus Iterative Learning Control (last iteration). The black point represents the frequency switching time.

are important in order to show that the ILC is able to achieve a stable behavior and converge to a constant error value. The rms tracking error, i.e. E_{rms}, was computed using the equation (5.25).

As the resonant gain scheduling controller is more complex than the proportional-integral one, the ILC required more iterations in order to achieve a constant error value. Although the errors dynamics are more erratic than the ones found in the comparative controller, they proved to converge after approximately 260 iterations.

Figure 26 – RAS x and y axes rms error over the iterations for the resonant gain scheduling controller.

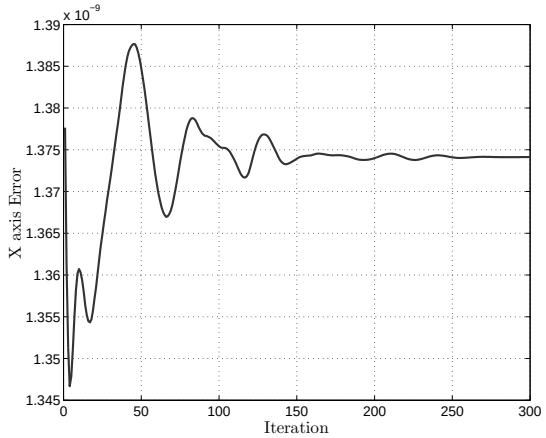

(a) X axis rms error over the iterations.

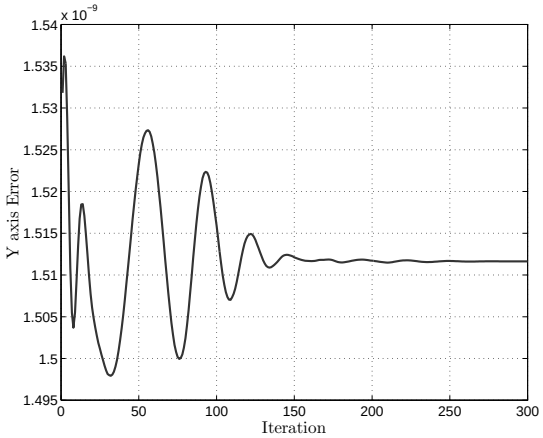

(b) Y axis rms error over the iterations.

5.7 Performance for Higher Velocity

In order to further demonstrate the resonant gain scheduling controller performance, a simulation was performed for a reference with higher velocity values. Now, the RAS pattern is given by the following parameters: radius $R_s = 1\mu$m, spiral total time $T = 0.00148s$, switching time $t_{*0} = 1.55 \times 10^{-4}s$, constant linear velocity $v = 0.0223m/s$ and constant angular velocity of $\omega = 15000\pi$. This value is two times higher than the reference pattern used in Bazaei, Maroufi e Moheimani (2017), that is the only work regarding the control of the OPT pattern (ZIEGLER et al., 2017).

Figure 27 presents the output responses, for the previously defined spiral, for both the PI and the resonant gain scheduling controllers. As it is possible to see, the faster RAS pattern reduced the tracking performance of both controllers, as the frequency values become too higher in order to be properly tracked. Nevertheless, the proposed controller is still able to deliver a better response than the proportional-integral controller, with the main drawback localized at the center of the spiral.

Figure 27 – RAS spiral reference and output responses, between $\pm 1.1\mu$, for a higher velocity with both controllers. The black point represents the frequency switching time.

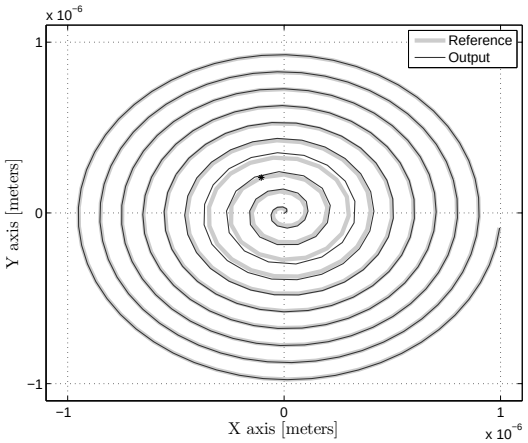

(a) RAS spiral reference and output responses for the resonant gain scheduling controller.

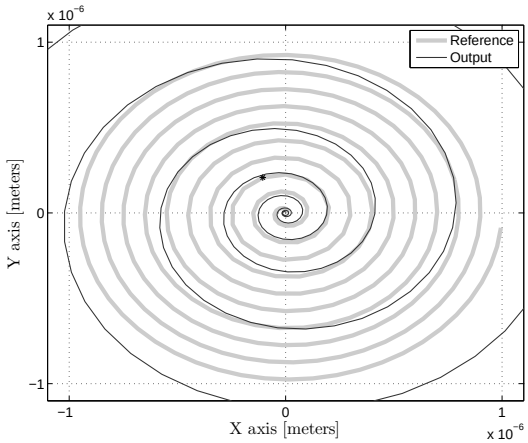

(b) RAS spiral reference and output responses for the proportional-integral controller.

5.8 Final Considerations

This chapter presented the main results obtained by this dissertation proposal: the resonant gain scheduling controller. In order to stablish a performance comparison with the resonant gain scheduling controller, a proportional-integral controller, usual in Atomic Force Microscopes equipment, was also presented. Both controllers also received the addition of an Iterative Learning Control in order to improve the tracking performance. The results demonstrate the proposed controller superior performance in comparison to the comparative techniques.

So as to quantify the graphical results previously presented, the *rms* values of the tracking errors of the RAS pattern were computed. The *rms* tracking error E_{rms} was computed using the equation (5.25). For the complete spiral case, the error E_{rms} was computed using the following equation

$$E_{rms} = \sqrt{\frac{\sum_{i=1}^{N}((\mathbf{rx}_i - \mathbf{yx}_i)^2 + (\mathbf{ry}_i - \mathbf{yy}_i)^2)}{N}}, \tag{5.27}$$

where **rx**, **ry**, **yx** and **yy** are the reference and output signals vectors for the x and y axes, respectively.

The numerical results for the controllers regarding the RAS pattern are presented in Table 1. As it is possible to see, the proposed resonant gain scheduling controller achieved better results in comparison the comparative proportional-integral controller. It is important to notice that the ILC addition improved the performance of both strategies, mainly in the comparative one.

Table 1 – RMS error values for the RAS pattern of both controllers.

	Proposed Controller	Comparative Controller
	$E_{rms}(\times 10^{-8})$	$E_{rms}(\times 10^{-8})$
Without ILC	0.2315	15.93
With ILC (last iteration)	0.2295	12.52

Table 2 presents the numerical results for the components of the RAS pattern, detailing the rms error for both the x and y axes and their respective control inputs. The input signal u_{rms} was computed using a similar procedure that the rms error.

Table 2 – RMS error and input ($\times 10^{-7}$) values for the RAS pattern of both controllers for the x and y axes.

	Axes	Proposed Controller		Comparative Controller	
		E_{rms} $(\times 10^{-8})$	u_{rms}	$E_{rms}(\times 10^{-8})$	u_{rms}
Without ILC	x	0.13776	4.2458	10.146	4.9385
	y	0.15318	4.2399	10.138	4.9289
With ILC (last iteration)	x	0.13741	4.2454	7.9750	4.8914
	y	0.15116	4.2404	7.9760	4.8871

It is notable that the smaller rms error values of the proposed resonant gain scheduling controller do not require bigger control inputs when compared to the proportional-integral controller. This is due to the proposed controller property of using the signal frequency dynamics into consideration for the input calculation.

Finally, the ILC control input two-norm convergence, as stated in Theorem 3.3, is presented in Figure 28 for the x axis. The y axis signals are very similar to the x axis ones. As it is possible to see, both controllers achieved the convergence stated in the Theorem.

Figure 28 – Two-norm of the ILC control input signals for the proportional-integral and the resonant gain scheduling controllers for the x axis.

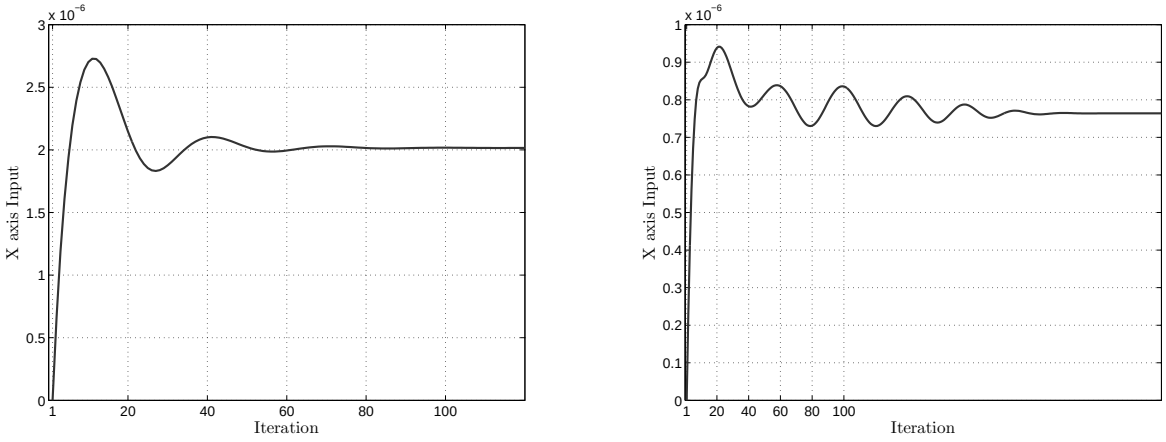

(a) Proportional-integral controller ILC control input two-norm.

(b) Resonant gain scheduling controller ILC control input two-norm.

6 Conclusions

This dissertation proposed a control structure in order to perform the tracking of frequency and amplitude-varying sinusoidal signals. These signals can be used in order to generate spiral patterns, which are reference signals used in different relevant applications, such as the Atomic Force Microscopy. In order to consider the variability in the reference parameters, which makes the direct application of the Internal Model Principle not suitable, the dissertation used a robust control strategy in an augmented framework. The system model and the reference parameters were structured as Linear Matrix Inequalities, which were solved as optimization problems.

In order to improve the tracking performance, the work also used feedforward control strategies, namely the system gain compensation and the Iterative Learning Control. Moreover, a Kalman Filter was designed so as to simulate the controller application in a real system, where only the output could be measured and the system states, necessary for the feedback controller, needed to be estimated. The proposed controller performance was compared to a proportional-integral controller, commonly found in atomic force microscopes, with a feedforward gain compensation and an Iterative Learning controller, projected in a similar way to the proposed controller.

In order to perform the simulations, a new scanning pattern, called Repetitive Arquimedean Spiral, was proposed. It consists, basically, in a mirrored version of the Optimal Archimedean Spiral, where now the spiral consists in a closed path. This pattern can be used in applications where the continuous scanning of the sample is necessary, such as in a video recording, where the spiral must be able to start and end in the same point using a smooth dynamic. As the scanning pattern is repeated multiple times, the Iterative Learning Control strategy was a suitable option.

A set of simulations were performed in order to demonstrate the performance of the proposed resonant gain scheduling controller. The graphical and numerical results demonstrated that the proposed controller obtained good results, being able to achieve satisfactory reference tracking. This is due to the resonant gain scheduling controller capacity of using the knowledge of the frequency value at each sample time. On the other hand, the proportional-integral controller is not adequate to perform this task, which generated inferior results. Although the proposed controller achieved better performance, it did no require bigger control efforts than the comparative one.

As expected, the Iterative Learning Control addition to both controllers improved the tracking performance, considering that the same scanning pattern must be tracked multiple times. The improvement could better be visualized for the proportional-integral

controller rather than the resonant gain scheduling controller. As the proposed controller already have a small tracking error, the comparative controller could benefit further by the ILC structure.

In conclusion, the dissertation objective was accomplished with the resonant gain scheduling controller. Different control strategies were presented, all of them studied in order to achieve satisfactory tracking of amplitude and frequency-varying sinusoidal signals. The numerical simulations, using a numerical model of a real system, demonstrated the dissertation ideas and procedures relevance.

6.1 Future Work Perspectives

For future works, the main perspective is the validation of the presented control structure in a real application. Besides the focus on Atomic Force Microscopes, which were the focus of the dissertation, there are other applications where this work may be suitable. It is possible to cite some examples as the Fiber Scanners (LEE et al., 2010), applied in the medical area in order to perform internal body imaging, and the Pico-Projectors (SCHOWENGERDT et al., 2009), used in modern smartphones and computers for image projecting and scanning.

Besides the satisfactory results presented in the dissertation, the Internal Model Principle stability guarantee is lost due to the reference time-varying properties. Nevertheless, the IMP has different application approaches that can be more suitable for the work problem. One example is the work presented by Isidori e Byrnes (1990), which uses a different approach of the Internal Model Principle. In order to give the main idea about this approach, let us consider the following differential equations:

$$\dot{x} = f(x, u) \tag{6.1a}$$

$$\dot{w} = s(w), \tag{6.1b}$$

where the first equation describes a system with states $x \in \mathbb{R}^n$ and input $u \in \mathbb{R}^m$, and the second one regards the reference signal, now generated by a so-called exosystem $w \in \mathbb{R}$.

According to Chen e Huang (2015), it is possible to design a control law that renders the system (6.1a) capable of tracking (6.1b), based on the existence of a determinate invariant manifold where the trajectories of the error will converge to zero as time tends to infinity. If there is such set, then a control law (ISIDORI; BYRNES, 1990)

$$u(w) = C(w) + Ke(w), \tag{6.2}$$

is able to render the manifold invariant, which is achieved by the $C(w)$ term, and able to annihilate the tracking error $e = (x - \pi(w))$. The term $\pi(w)$ is a mapping of x that

satisfies (ISIDORI; BYRNES, 1990)

$$\frac{\partial \pi}{\partial w} s(w) = f(\pi(w), u(w)), \tag{6.3}$$

where $f(\pi(w), u(w))$ is the augmented system, such as proposed by the original IMP.

The presented ideas are suitable for the OPT spiral problem, if we consider that the amplitude and frequency-varying sinusoidal signals are references that can be represented as appropriate exosystems.

A further study on the feedforward control strategies, such as the reviewed Iterative Learning Control, is also an interesting point. Considering the present dissertation application, where the Atomic Force Microscopy scanners may perform tasks multiple times with the same scanning pattern, the Iterative Learning Control emerges as a suitable option. The simulation results demonstrated the control strategy potential in the performance increasing of spiral patterns tracking. For future works, a further study on the design of the Q-filter and the learning function is suggested, as these structures are the main parts of the Iterative Learning Control and can be designed using different approaches. For example, one may suggest an ILC design through an optimization problem structured using LMIs, such as the one used in the Resonant Gain Scheduling controller design.

Bibliography

ABRAMOVITCH, D. Y. et al. A Tutorial on the Mechanisms, Dynamics, and Control of Atomic Force Microscopes. In: *2007 American Control Conference*. [S.l.]: IEEE, 2007. p. 3488–3502. ISBN 1-4244-0988-8. ISSN 0743-1619. Cited in page 29.

BARÓ, A. M.; REIFENBERGER, R. G. (Ed.). *Atomic Force Microscopy in Liquid Biological Application*. Weinheim, Germany: Wiley-VCH Verlag GmbH & Co. KGaA, 2012. ISBN 9783527649808. Cited 5 times in pages 15, 27, 28, 29, and 53.

BAZAEI, A. et al. Internal Model Control for Spiral Trajectory Tracking With MEMS AFM Scanners. *IEEE Transactions on Control Systems Technology*, v. 24, n. 5, p. 1717–1728, sep 2016. ISSN 1063-6536. Cited 2 times in pages 15 and 51.

BAZAEI, A.; MAROUFI, M.; MOHEIMANI, S. R. Tracking of constant-linear-velocity spiral trajectories by approximate internal model control. In: *2017 IEEE Conference on Control Technology and Applications (CCTA)*. [S.l.]: IEEE, 2017. p. 129–134. ISBN 978-1-5090-2182-6. Cited 4 times in pages 16, 33, 51, and 69.

BAZAEI, A.; YONG, Y. K.; MOHEIMANI, S. O. R. *High-speed Lissajous-scan atomic force microscopy: Scan pattern planning and control design issues*. 2012. Cited in page 30.

BERNUSSOU, J.; PERES, P.; GEROMEL, J. Stabilizability of Uncertain Dynamical Systems: The Continuous and the Discrete Case. *IFAC Proceedings Volumes*, Elsevier, v. 23, n. 8, p. 159–164, aug 1990. ISSN 1474-6670. Cited 3 times in pages 17, 21, and 22.

BOEREN, F. et al. Frequency-Domain ILC Approach for Repeating and Varying Tasks: With Application to Semiconductor Bonding Equipment. *IEEE/ASME Transactions on Mechatronics*, v. 21, n. 6, p. 2716–2727, dec 2016. ISSN 1083-4435. Cited 4 times in pages 17, 40, 41, and 55.

BOYD, S. P. *Linear matrix inequalities in system and control theory*. [S.l.]: Society for Industrial and Applied Mathematics, 1994. 193 p. ISBN 089871334X. Cited 3 times in pages 17, 24, and 45.

BRISTOW, D.; THARAYIL, M.; ALLEYNE, A. A survey of iterative learning control. *IEEE Control Systems Magazine*, v. 26, n. 3, p. 96–114, jun 2006. ISSN 0272-1708. Cited 5 times in pages 17, 35, 36, 40, and 41.

BUTTERWORTH, J. A.; PAO, L. Y.; ABRAMOVITCH, D. Y. A comparison of ilc architectures for nanopositioners with applications to afm raster tracking. In: *Proceedings of the 2011 American Control Conference*. [S.l.: s.n.], 2011. p. 2266–2271. ISSN 0743-1619. Cited in page 17.

CHEN, C. T. *Linear System Theory and Design*. 1999. 334 p. Cited 5 times in pages 16, 24, 38, 42, and 48.

CHEN, Z.; HUANG, J. *Stabilization and Regulation of Nonlinear Systems*. Cham: Springer International Publishing, 2015. (Advanced Textbooks in Control and Signal Processing). ISBN 978-3-319-08833-4. Cited in page 73.

DAS, S. K.; POTA, H. R.; PETERSEN, I. R. Resonant controller for fast atomic force microscopy. In: *2012 IEEE 51st IEEE Conference on Decision and Control (CDC)*. [S.l.]: IEEE, 2012. p. 2471–2476. ISBN 978-1-4673-2066-5. Cited in page 16.

DUAN, G.; YU, H.-H. *LMIs in control systems : analysis, design and applications*. [S.l.]: CRC Press, 2013. ISBN 9781466582996. Cited 2 times in pages 21 and 24.

FRANCIS, B.; WONHAM, W. The internal model principle of control theory. *Automatica*, v. 12, n. 5, p. 457–465, sep 1976. ISSN 00051098. Cited 3 times in pages 16, 24, and 25.

HABIBULLAH, H.; POTA, H.; PETERSEN, I. Phase-locked loop-based proportional integral control for spiral scanning in an atomic force microscope. *IFAC Proceedings Volumes*, v. 47, n. 3, p. 6563 – 6568, 2014. ISSN 1474-6670. 19th IFAC World Congress. Cited in page 53.

HABIBULLAH, H.; POTA, H. R.; PETERSEN, I. R. High-speed spiral imaging technique for an atomic force microscope using a linear quadratic Gaussian controller. *Review of Scientific Instruments*, American Institute of PhysicsAIP, v. 85, n. 3, p. 033706, mar 2014. ISSN 0034-6748. Cited 2 times in pages 15 and 16.

ISIDORI, A.; BYRNES, C. Output regulation of nonlinear systems. *IEEE Transactions on Automatic Control*, v. 35, n. 2, p. 131–140, 1990. ISSN 00189286. Cited 2 times in pages 73 and 74.

JIN, X. Non-repetitive trajectory tracking for joint position constrained robot manipulators using iterative learning control. In: *2016 IEEE 55th Conference on Decision and Control (CDC)*. [S.l.: s.n.], 2016. p. 5490–5495. Cited in page 15.

KALMAN, R. E. A new approach to linear filtering and prediction problems. *Transactions of the ASME–Journal of Basic Engineering*, v. 82, n. Series D, p. 35–45, 1960. Cited in page 26.

KHALIL, H. *Nonlinear systems (3rd) Prentice Hall*. [S.l.: s.n.], 2002. Cited in page 19.

LEE, C. M. et al. Scanning fiber endoscopy with highly flexible, 1 mm catheterscopes for wide-field, full-color imaging. *Journal of biophotonics*, NIH Public Access, v. 3, n. 5-6, p. 385–407, jun 2010. ISSN 1864-0648. Cited 2 times in pages 15 and 73.

LIN, C. J.; WU, C. H.; HWANG, C. C. Tracking control of a motor-piezo xy gantry using a dual servo loop based on ilc and ga. In: *2009 IEEE International Conference on Control and Automation*. [S.l.: s.n.], 2009. p. 1098–1103. ISSN 1948-3449. Cited in page 17.

LOFBERG, J. YALMIP : a toolbox for modeling and optimization in MATLAB. In: *2004 IEEE International Conference on Robotics and Automation (IEEE Cat. No.04CH37508)*. [S.l.]: IEEE, 2004. p. 284–289. ISBN 0-7803-8636-1. Cited in page 50.

MAHMOOD, I. A.; MOHEIMANI, S. O. R. Spiral-scan Atomic Force Microscopy: A constant linear velocity approach. In: *10th IEEE International Conference on Nanotechnology*. [S.l.]: IEEE, 2010. p. 115–120. ISBN 978-1-4244-7033-4. Cited 3 times in pages 15, 16, and 31.

MAHMOOD, I. A.; MOHEIMANI, S. O. R.; BHIKKAJI, B. A new scanning method for fast atomic force microscopy. *IEEE Transactions on Nanotechnology*, v. 10, n. 2, p. 203–216, 2011. ISSN 1536125X. Cited 3 times in pages 15, 29, and 30.

MAROUFI, M.; MOHEIMANI, S. O. R. A 2DOF SOI-MEMS Nanopositioner With Tilted Flexure Bulk Piezoresistive Displacement Sensors. *IEEE Sensors Journal*, v. 16, n. 7, p. 1908–1917, apr 2016. ISSN 1530-437X. Cited 2 times in pages 29 and 51.

MEYER, E.; HUG, H. J.; BENNEWITZ, R. *Scanning Probe Microscopy : the Lab on a Tip*. [S.l.]: Springer Berlin Heidelberg, 2004. 210 p. ISBN 9783662098011. Cited 3 times in pages 28, 29, and 53.

MONTAGNER, V. F.; PERES, P. L. D. State feedback gain scheduling for linear systems with time-varying parameters. In: *Proceedings of the 2004 American Control Conference*. [S.l.: s.n.], 2004. v. 3, p. 2004–2009 vol.3. ISSN 0743-1619. Cited in page 23.

NORRLOF, M.; GUNNARSSON, S. Time and frequency domain convergence properties in iterative learning control. *International Journal of Control*, Taylor & Francis Group, v. 75, n. 14, p. 1114–1126, jan 2002. ISSN 0020-7179. Cited 3 times in pages 35, 37, and 38.

OGATA, K. *Discrete-time control systems*. [S.l.]: Prentice-Hall, 1987. 994 p. ISBN 9780132161022. Cited in page 26.

OLIVEIRA, M. de; SALTON, A. T.; FLORES, J. F. Controle ressonante ótimo de frequência variável para escaneamento espiral em microscopia de força atômica. In: *Simpósio Brasileiro de Automação Inteligente (SBAI) 2017*. [S.l.]: SBAI, 2017. p. 497–502. ISSN 2175-8905. Cited in page 16.

OWENS, D. H. *Iterative learning control : an optimization paradigm*. [S.l.: s.n.], 2015. 456 p. ISBN 9781447167709. Cited 3 times in pages 35, 36, and 38.

PEREIRA, L. F. A. et al. Multiple resonant controllers for uninterruptible power supplies – a systematic robust control design approach. *IEEE Transactions on Industrial Electronics*, v. 61, n. 3, p. 1528–1538, March 2014. ISSN 0278-0046. Cited in page 16.

RAMOS, G. A.; SOTO-PEREZ, R. A.; CIFUENTES, J. A. A Varying Frequency LPV-Based Control Strategy for Three-Phase Inverters. *IEEE Transactions on Industrial Electronics*, v. 64, n. 9, p. 7599–7608, sep 2017. ISSN 0278-0046. Cited in page 15.

RANA, M. S.; POTA, H. R.; PETERSEN, I. R. Spiral Scanning With Improved Control for Faster Imaging of AFM. *IEEE Transactions on Nanotechnology*, v. 13, n. 3, p. 541–550, may 2014. ISSN 1536-125X. Cited 3 times in pages 15, 29, and 30.

RANA, M. S.; POTA, H. R.; PETERSEN, I. R. Performance of Sinusoidal Scanning With MPC in AFM Imaging. *IEEE/ASME Transactions on Mechatronics*, v. 20, n. 1, p. 73–83, feb 2015. ISSN 1083-4435. Cited in page 16.

SCHOWENGERDT, B. T. et al. 1-mm diameter, full-color scanning fiber pico projector. v. 40, 06 2009. Cited 3 times in pages 15, 16, and 73.

THRUN, S.; BURGARD, W.; FOX, D. *Probabilistic robotics*. [S.l.]: MIT Press, 2005. 647 p. ISBN 0262201623. Cited 2 times in pages 26 and 27.

TOH, K. C.; TODD, M. J.; TUTUNCU, R. H. SDPT3 - A Matlab software package for semidefinite programming, Version 1.3. *Optimization Methods and Software*, Gordon and Breach Science Publishers, v. 11, n. 1-4, p. 545–581, jan 1999. ISSN 1055-6788. Cited in page 50.

TSUKRUK, V. V.; SINGAMANENI, S. *Scanning probe microscopy of soft matter : fundamentals and practices.* [S.l.: s.n.], 2011. 664 p. ISBN 3527327436. Cited 3 times in pages 27, 28, and 51.

TUMA, T. et al. The Four Pillars of Nanopositioning for Scanning Probe Microscopy: The Position Sensor, the Scanning Device, the Feedback Controller, and the Reference Trajectory. *IEEE Control Systems*, v. 33, n. 6, p. 68–85, dec 2013. ISSN 1066-033X. Cited 2 times in pages 15 and 30.

WANG, Y.; CHU, K. C.; TSAO, T.-C. An analysis and synthesis of internal model principle type controllers. In: *2009 American Control Conference*. [S.l.]: IEEE, 2009. p. 488–493. ISBN 978-1-4244-4523-3. Cited in page 25.

WU, Y.; ZOU, Q. An iterative based feedforward-feedback control approach to high-speed AFM imaging. In: *2009 American Control Conference*. [S.l.]: IEEE, 2009. p. 1658–1663. ISBN 978-1-4244-4523-3. Cited 2 times in pages 17 and 41.

WU, Y.; ZOU, Q.; SU, C. A Current Cycle Feedback Iterative Learning Control Approach for AFM Imaging. *IEEE Transactions on Nanotechnology*, v. 8, n. 4, p. 515–527, jul 2009. ISSN 1536-125X. Cited 2 times in pages 17 and 53.

YABLON, D. G. *Scanning Probe Microscopy for Industrial Applications : Nanomechanical Characterization.* [S.l.]: Wiley, 2014. ISBN 1118288238. Cited 4 times in pages 15, 28, 29, and 50.

YONG, Y. K.; MOHEIMANI, S. O. R.; PETERSEN, I. R. High-speed cycloid-scan atomic force microscopy. *Nanotechnology*, IOP Publishing, v. 21, n. 36, p. 365503, sep 2010. ISSN 0957-4484. Cited in page 30.

ŻAK, S. H. *Systems and Control*. New York: Oxford University Press, 2003. 704 p. ISBN 0195150112. Cited 2 times in pages 17 and 53.

ZIEGLER, D. et al. Ideal Scan Path for High-Speed Atomic Force Microscopy. *IEEE/ASME Transactions on Mechatronics*, v. 22, n. 1, p. 381–391, feb 2017. ISSN 1083-4435. Cited 6 times in pages 16, 30, 32, 33, 51, and 69.

Pontifícia Universidade Católica do Rio Grande do Sul
Pró-Reitoria de Graduação
Av. Ipiranga, 6681 - Prédio 1 - 3º. andar
Porto Alegre - RS - Brasil
Fone: (51) 3320-3500 - Fax: (51) 3339-1564
E-mail: prograd@pucrs.br
Site: www.pucrs.br